Bubble vent localization for marine hydrocarbon seep surveys

Garrett A. Mitchell[1], Larry A. Mayer[2], and Jamshid J. Gharib[3]

Abstract

Commercial success of marine seep hunting exploration campaigns involves acquisition of high-quality bathymetry and backscatter along with targeted coring of shallow geochemical sampling of seep sediments. The sharp lateral chemical gradient encompassing seafloor seeps requires accurate identification of seep sites from high-resolution acoustic data. Active seafloor seeps featuring plumes of gas bubbles and oil droplets rising into the water column can be imaged with modern multibeam echosounders providing an effective approach to remotely characterizing seafloor seeps. Interpreting the seafloor position of gas plume emissions in multibeam data using existing mapping methodology is hindered by slow processing due to large files sizes, a manual "by eye" qualitative assessment of each sonar ping searching for plume anomalies, skill and fatigue of the geoscientist, and environmental or acquisition artifacts that can mask the precise location of gas emission on the seafloor. These limitations of midwater backscatter mapping create a qualitative data set with varying inherent positional errors that can lead to missed or incorrect observations about seep-related seafloor features and processes. By vertically integrating midwater multibeam amplitude samples, a 2D midwater backscatter raster can be generated and draped over seafloor morphology, providing a quantitative synoptic overview of the spatial distribution of gas plume emission sites for more refined seafloor interpretation. We reprocess multibeam midwater data set from NOAA Cruise EX1402L2 in the northwestern Gulf of Mexico using a vertical amplitude stacking technique. Constructed midwater backscatter surfaces are compared with digitized plume positions collected during the survey for a comparison into assessing uncertainty in mapping approaches. Our results show that the accuracy of manually digitizing gas emission sites varies considerably when compared with the midwater backscatter amplitude maps. This quantitative plume mapping technique offers multiple advantages over traditional geopicking from cost effectiveness, offshore efficiency, repeatability, and higher accuracy, ultimately improving the detectability and sampling of active seafloor seeps through precisely located cores.

Introduction

Seep hunting for seafloor geochemical exploration surveys

Marine seep hunting surveys and geochemical evaluation of seep sediments are an important hydrocarbon exploration tool helping to reduce exploration risk and cost in prospective frontier basins. Seafloor geochemical exploration programs are designed based on the observations that buoyant hydrocarbon-rich liquids, generated by the deep burial and heating of kerogen-containing source rock, percolate to the seafloor and can be sampled from seafloor and shallow subsurface sediments and analyzed to evaluate commercial potential. Geochemical analyses of hydrocarbon fluids in calibration tests show robust association between deep commercial reservoirs and seafloor seeps (Abrams and Dahdah, 2011). Near-surface seepage contains geochemical fingerprints that provide insight into age and maturity, source rock type, depositional and thermal history, and ultimately commercial potential of deep hydrocarbon reservoir (Abrams, 2005). Identifying and sampling sites where deep fluids have migrated to the seafloor provides high-quality geochemical data for assessing and modeling deep hydrocarbon reservoirs.

Because oil exploration moved from land to the challenging deepwater marine environment, locating and sampling seafloor and shallow seep sediments offshore has progressed with the development of innovative marine geophysical tools (i.e., subsea navigation) and geochemical techniques (i.e., onboard geochemistry). Modern marine seep hunting surveys use seismic and multibeam echosounder (MBES) technology to

[1]Fugro USA Marine Inc., Houston, Texas 77081, USA and University of New Hampshire, Center for Coastal and Ocean Mapping, Durham, New Hampshire 03824, USA. E-mail: gmitchell@fugro.com (corresponding author).

[2]University of New Hampshire, Center for Coastal and Ocean Mapping/Joint Hydrographic Center, Durham, New Hampshire 03824, USA. E-mail: larry@ccom.unh.edu.

[3]Fugro USA Marine Inc., Houston, Texas 77081, USA. E-mail: jgharib@fugro.com.

Manuscript received by the Editor 11 April 2021; revised manuscript received 5 November 2021; published online 26 January 2022. This paper appears in *Interpretation*, Vol. 10, No. 1 (February 2022); p. SB107–SB128, 32 FIGS., 2 TABLES.

http://dx.doi.org/10.1190/INT-2021-0084.1.

DOI:10.1190/INT-2021-0084.1

help locate suitable coring locations based on specific acoustic responses characteristic of various geologic features associated with seafloor seepage. Specifically, the identification of deep-seated faults that facilitate fluid migration to the seafloor and the expression of hydrocarbon seep environments that can include fluid expulsion features such as pockmarks and mud volcanoes; authigenic carbonate hardgrounds and crusts; and biological indicators like chemosynthetic communities, gas bubbles, and oil droplets in the water column (Figure 1).

Multibeam mapping of hydrocarbon seeps

In offshore seep hunting, MBESs play a key role in detecting and characterizing areas of active and relic seafloor seepage (Orange et al., 2010; Weber et al., 2014; Mitchell et al., 2018). Low-frequency multibeam sonars (12–30 kHz) can cover large swaths of deep seafloor per day (1500 km^2) searching for acoustic signatures of seep-related features on the seafloor and in the water column. MBES surveys generate three primary acoustic data sets that can be used for locating active and relic seepage (Figure 2). Bathymetry provides depth and morphological data that include bathymetric highs associated with mud volcanoes and expulsion mounds, topographic lows associated with pockmarks, and seafloor faults that serve as petroleum fluid migration pathways (Figure 2a). Seafloor backscatter, a measure of backscattered acoustic energy from the seafloor, can detect seep-related authigenic carbonate deposits, chemosynthetic communities and shell debris, gassy muds, and brine pools (Figure 2b). Midwater backscatter can detect free gas release from seafloor venting that expels clusters of oil and gas bubbles thousands of meters into the water column (Figure 2c) (Römer et al., 2012).

The integration of MBES-derived data sets with sub-bottom profiler data provides a powerful interpretive tool to identify, characterize, and rank seafloor fluid emission sites for geochemical sampling surveys. Core target positions on interpreted seafloor seeps are initially chosen and characterized from the data in near real time using a geographic information system (GIS) environment, ranked by geoscientists based on various criteria using observed seep-related geophysical proxies at each site (i.e., areas of seafloor with discrete anomalously high seafloor backscatter near a fault would be considered a relatively high-ranking target; a similar target with a detected plume even higher), then precisely sampled using ultrashort baseline (USBL) assisted navigation technology.

Seafloor seeps are small, discrete, and transient features. The geochemical signal of sediment near seeps has a steep lateral chemical gradient (Abrams, 1996, 2005). Missing a coring target on the order of 10 m may result in a negative geochemical result leading to flawed conclusions about the commercial potential of the reservoir (McConnell and Orange, 2014). Locating the highest quality geochemical data necessary for understanding characteristics of the deep reservoir directly depends on good quality high-resolution geophysical data, subsea acoustic positioning, and proper interpretation based on integration of the acoustic data sets.

Water column imaging of bubble plumes

Water column imaging MBES has been shown to be valuable exploration tools for the detection and

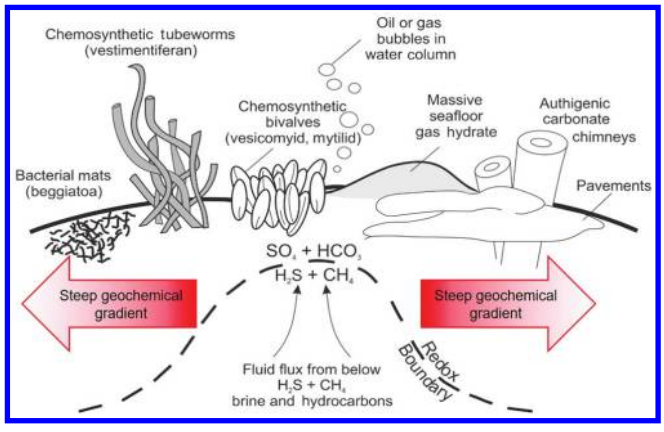

Figure 1. Simplified schematic of a hydrocarbon seep, geochemistry, and associated seep features (adopted from McConnell and Orange, 2014).

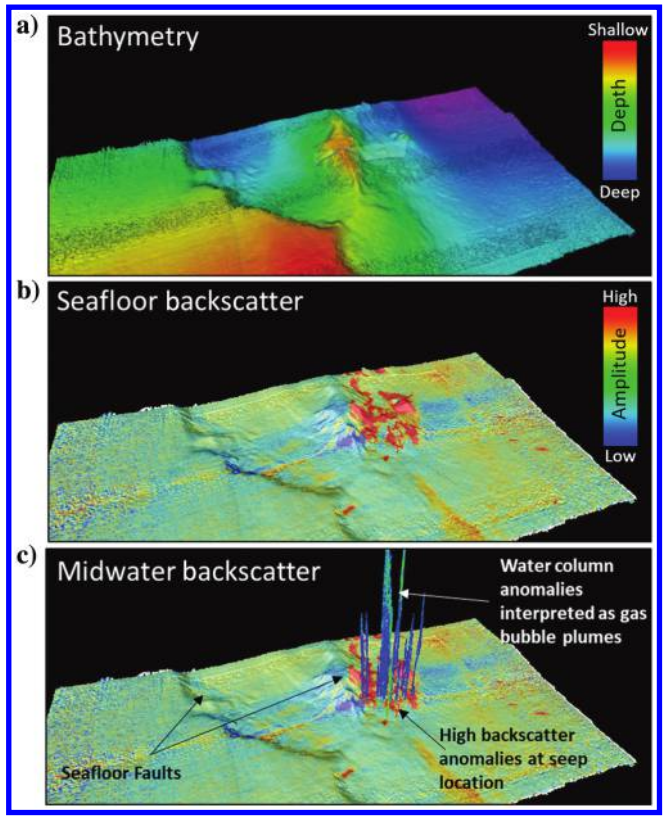

Figure 2. Multibeam-derived data sets used for seep hunting. (a) Bathymetry from multibeam data is used to identify seep-related morphologic features. (b) Seafloor backscatter data are superimposed over bathymetry and assists in identifying high-potential seep targets (high acoustic reflectivity associated with carbonate slabs, crusts, and chemosynthetic fauna/shell fragments). (c) Water column information helps fine tune and rank high-potential seep targets by revealing midwater acoustic backscatter anomalies characteristic of gas plumes.

DOI:10.1190/INT-2021-0084.1

identification of entrained bubble plumes (mapping spatial distribution and vertical extent of bubble plumes) over extensive areas of seafloor (Schneider von Deimling et al., 2007; Nikolovska et al., 2008; Weber et al., 2012; Skarke et al., 2014). Within the past 10 years, MBES has been upgraded to record the time series for each beam providing backscatter amplitude measurements of the water column. Acoustic sensing of water column scattering properties has long been used by the fisheries community for fish stock and biomass assessments (Trenkel et al., 2008; Korneliussen et al., 2009; Innangi et al., 2016). The frequency range of the MBES used in deepwater seep surveying (12–30 kHz) emits wide swaths (5 × 7 times water depth) of acoustic beams that can reliably detect plumes of bubbles with diameters of 2–5 mm over 1500 km^2 of seafloor per day. Methane bubbles, specifically gas bubbles covered with a thin gas hydrate shell (Brewer et al., 1998), have a very strong acoustic impedance contrast with respect to the surrounding seawater and appear as bright, semivertically oriented reflectors in successive across-track echogram images. MBES water column imaging shows that the bubbles can rise more than 2000 m off the seafloor (Römer et al., 2012) indicating that the bubble dissolution does not occur rapidly under certain conditions, most likely due to the hydrate coatings surrounding the methane bubble. The emission sites of free gas expulsion into the water column vary in time and space and are difficult to accurately locate using current manual mapping methodologies used in standard seep hunting surveys (Jerram et al., 2015). Due to this existing lack of fine-scale localization of active venting, the current intrinsic value in detection of bubble plumes during seep surveys is that they validate remote interpretation of seafloor amplitude patterns characteristic of seeps and help focus the interpreter to an area of potential seepage. It is important to note that an echogram is a snapshot of gas release in time and can therefore be used to investigate the temporal variability of seep's activity or quiescence.

Processing and visualization workflows of MBES midwater data during commercial seep hunting surveys have remained static since the inception of the technology. Primary processing and analysis software for commercial seep detection is Fledermaus Midwater (FMMidwater) developed by Quality Positioning Services (QPS). This current commercial workflow is shown in Figure 3. In FMMidwater, raw Kongsberg multibeam files from low-frequency MBES systems (*.all/*.wcd) are converted into a generic water column (*.gwc) format. Each *.gwc file is viewed in a side R-Stack (lateral range stacking technique) for a quick reconnaissance of data quality and major plumes (Figure 3a) before viewing the entire *.gwc file in a ping-by-ping beam fan view for anomalies interpreted to be bubble plumes. Prudent interpreters view this single ping view alongside a lateral stacked beam fan view to increase a bubble plume anomaly's signal (Figure 3b). Once an acoustic anomaly characteristic of a gas plume is detected in an echogram (plumes appear as acoustic semivertical reflectors with high backscatter values observed over multiple pings), the seafloor emission site is manually digitized as an *.xyz vector point in the single ping beam fan view window. Although this manual geopicking is the fastest option to interpret plume emission sites in midwater data for near real-time interpretation offshore, it is subjected to several sources of varying uncertainty that can interfere with interpreting the true position of seafloor gas expulsion. These manual geopicks are then interpreted in a 2D GIS and 3D QPS Fledermaus environment to examine the interpreted bubble source in context of the bathymetry and seafloor backscatter to determine optimal coring locations for geochemical sampling (Figure 3c).

Limitations of the current workflow

MBES generates vast amounts of data when recording the entire water column, which can pose logistic, economic, and technical challenges during geophysical data acquisition on seep surveys (Portell et al., 2019). Deepwater acquisition of a Kongsberg EM302 in

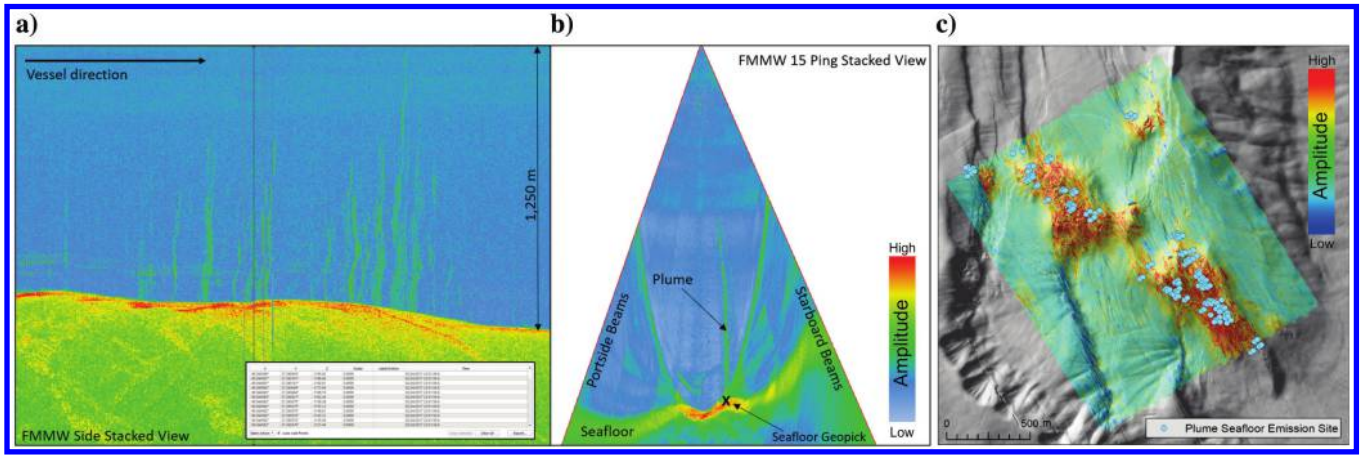

Figure 3. The MBES midwater mapping workflow commonly used in industry. (a) Side ranged stacked and (b) ping stacked images from FMMidwater software of plumes in Green Canyon Block 600, GOM. (c) Plume locations can be manually mapped ("geopicked") into xyz files that can be viewed in a GIS for analysis.

dual-ping Deep Mode creates approximately 300 MB *.all file and approximately 1.2 GB *.wcd file every 2 h during seep hunting surveys in water depths of 2000–3500 m. This large file size created when measuring full water column reflectivity makes remote data transmission off the vessel prohibitive with current technology and bandwidth limitations and water column data must be processed and interpreted offshore by geoscientists.

The immense volume of water column data acquired must be manually examined on a ping-by-ping basis for amplitude anomalies characteristic of midwater bubble plumes during seep surveys. This manual scrutiny often takes half of a typical offshore 12 h shift using this technique. Acquisition-related systematic and weather-related noise can interfere with manual analysis of data and existing quantitative methods that rely on a high signal-to-noise ratio (S/N) to extract high-amplitude discrete samples. With little swath overlap on adjacent survey lines and relatively fast survey speeds common in exploratory seep surveying, extra manual inspection is required within the noisy outer beam region dominated with sidelobe artifacts and low S/N to detect vertical bubble plumes within the echogram.

Exported geopicks interpreted to be the seafloor location of gas bubble emission sites are then analyzed in the context of other geophysical data sets to characterize active areas of hydrocarbon seepage for USBL-guided coring. Although this simple qualitative digitizing is commonly used by offshore seep geoscientists, the position of these point vectors that were traditionally mapped by eye can be a significant and often unaccounted for source of error (that may or may not be apparent to the interpreter and client). Water column sound speed refraction errors (Jerram et al., 2015), offshore sea state, vessel speed and heading, environmental or sensor noise that can significantly blur the precise location of gas emission on the seafloor, skill and fatigue of the offshore interpreter, and large file sizes all potentially deter precise and accurate digitization of gas emission sites within the data. Manual point digitizing along the semivertical plume introduces lateral errors that can be compounded by "ghost plumes." These MBES fore-aft transmitter sidelobe artifacts are created by strong scattering plumes. Ultimately, these by eye qualitative assessments of each sonar ping searching for plume anomalies lack repeatability. The subjectivity of these manually digitized single point seafloor gas emission sites often is lost when viewing in the context of the other quantitative surfaces derived from MBES such as hill-shaded relief and bathymetry, slope maps, and seafloor backscatter raster surfaces.

Although the simple presence of a bubble plume point in the GIS does not indicate a seep's potential thermogenic origins or sediment geochemistry, their observation within the survey area often invokes an excitement among clients considering that it is a relatively recent (decadal speaking) data set used as a seep indicator. The location of an interpreted point representing an emission source in the GIS project often becomes a high-ranking core target with little consideration into the inherent error in the interpreted seafloor position and the natural ephemerality of plumes. A skilled geoscientist will know that plumes tend to cluster, are typically, but not always near features such as seafloor faults, positive and negative relief expulsion features, and usually emanating from anomalously high seafloor reflectivity. A single digitized plume point can help increase the rank of a possible coring target; a point lacking these seep-related features should not be considered as a high-value target by itself.

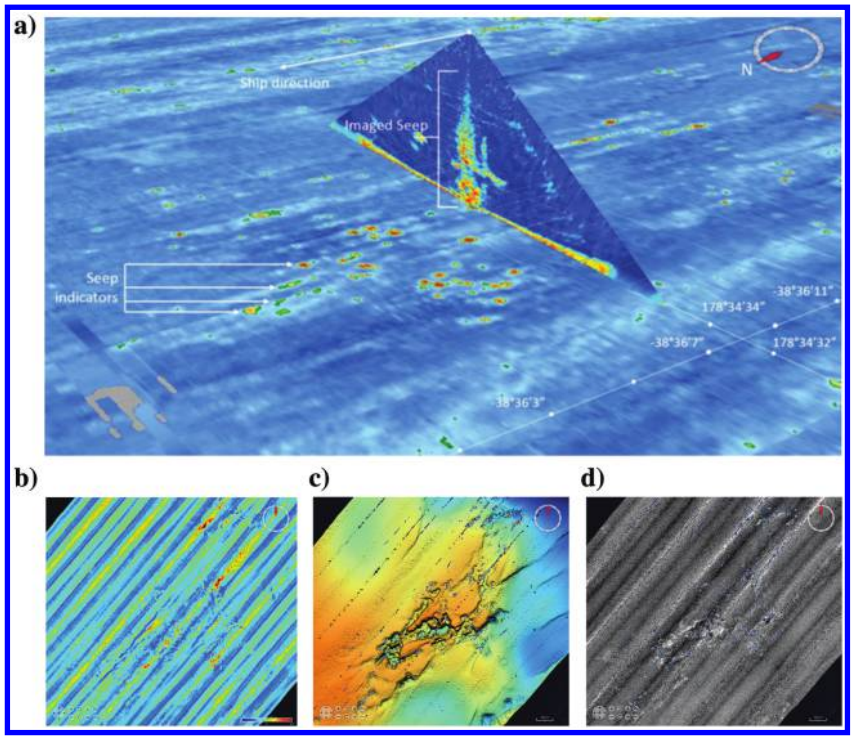

Figure 4. Data examples of EI using SonarScope software. The tool vertically integrates midwater backscatter amplitude from a user-specified percentage of water depth to create a 2D backscatter surface of midwater samples. The spatial distribution of plumes can be viewed in context with underlying bathymetry and seafloor backscatter through GIS layers, amplitude thresholding, and transparency. (a) Perspective view of draped EI surface showing high amplitude areas that correspond to midwater plumes observed in ping fan view. (b) Full coverage vertically integrated 2D midwater data mosaic. (c) Multibeam bathymetry with isolated high amplitude echo integrated anomalies created from amplitude thresholding showing the relationship between seafloor morphology with areas of gas emission and (d) isolated high amplitude integrated midwater anomalies in context of seafloor reflectivity. Images of Calypso hydrothermal vent field courtesy of NIWA/Ifremer.

DOI:10.1190/INT-2021-0084.1

DOI:10.1190/INT-2021-0084.1

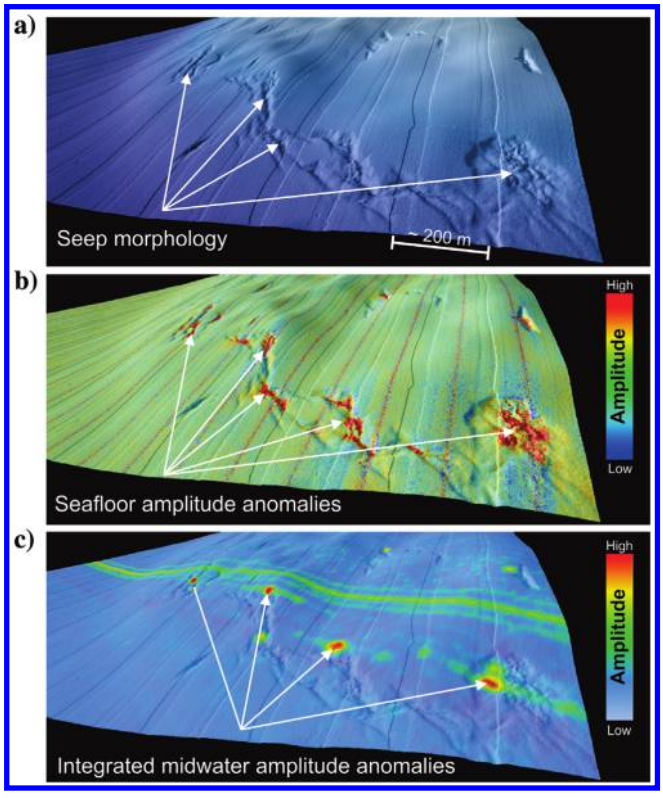

Figure 5. Geovisualization of the northwestern flank on Gloria Dome within Mississippi Canyon (MC) Block 297 using (a) 1 m bathymetry and (b) seafloor backscatter from a near-seafloor Kongsberg EM2000 (200 kHz) AUV survey with 5 m echo integrated midwater backscatter data from a Kongsberg EM302 (c) from National Oceanic and Atmospheric Administration (NOAA) Survey EX1105 data. Fine-scale AUV data overlain by hull-mounted EM302 midwater data show the close relationship among seep-related seafloor morphology, high seafloor reflectivity, and the location of active bubble vents. Data courtesy of National Institute for Undersea Science and Technology (NIUST) and NCEI, Boulder, CO.

Vertical stacking of midwater data

To improve localization of seafloor sources of hydrocarbon fluid emission, a vertical amplitude stacking technique derived from an existing fisheries echosounding method called echo integration (EI) can be applied to multibeam midwater data sets (Dragesund and Olsen, 1964; Simmonds and Maclennan, 2008; Dupré et al., 2015; Urban et al., 2017; Lamarche, 2019). EI of multibeam sonar data is a functionality of SonarScope, a MATLAB-based MBES diagnostic tool developed by Ifremer (Augustin, 2011). This mapping technique vertically integrates the acoustic amplitude samples from a set percentage or range of water depths and projects the resulting amplitude integration onto a 2D surface. This produces a backscatter image that can be viewed in context with bathymetry and seafloor reflectivity for refined seep characterization (Figure 4). As plumes of buoyant gas bubbles and oil droplets

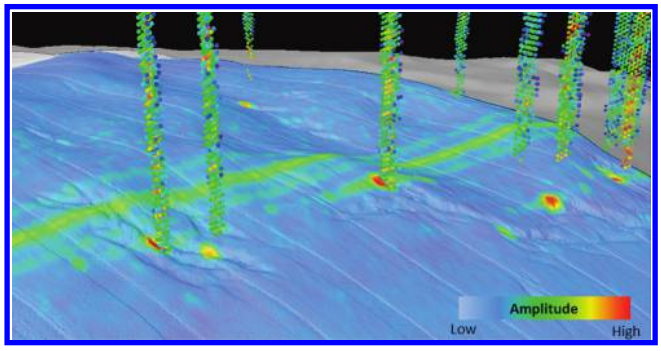

Figure 6. Perspective view of the northwestern flank on Gloria Dome within MC Block 297 showing correlation between quantitatively extracted plume point clouds colored by acoustic amplitude with 5 m echo integrated midwater backscatter data from a Kongsberg EM302.

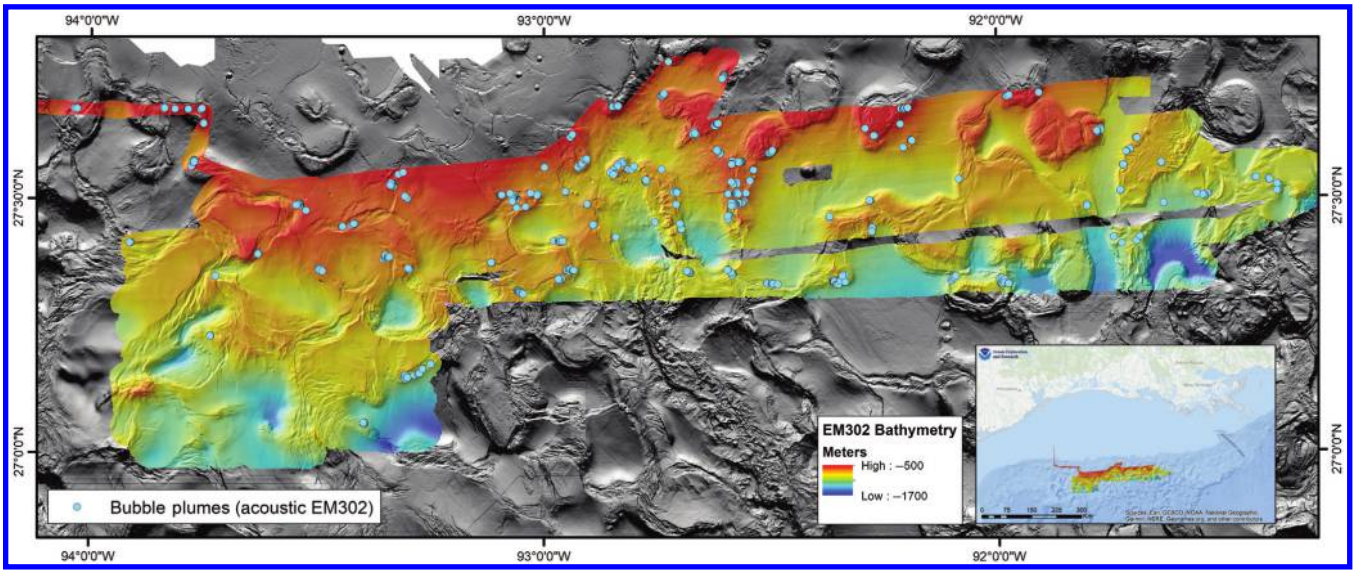

Figure 7. Study area of mapping operations during NOAA cruise EX1402L2. A primary scientific objective of this mapping is to identify cold seeps and chemosynthetic communities. During mapping operations, 695 plumes were manually identified in multibeam midwater data by NOAA.

ascend through the water column, they are subjected to varying lateral deflection due to currents. However, a vertical integration of midwater amplitude samples over a relatively narrow depth slice (typically 85%–96% of water depth) imprints a distinct bright amplitude anomaly in the backscatter raster that signifies the integrated position of the plume within that specific depth range. This resulting 2D midwater backscatter mosaic process can be automated to provide a synoptic view of the spatial distribution of hydrocarbon plume emission sites for interpreting seafloor seepage in the context of bathymetric and seafloor backscatter data sets (Figure 5). Figure 6 shows the close correlation between these vertically stacked amplitude anomalies with ascending bubble plumes.

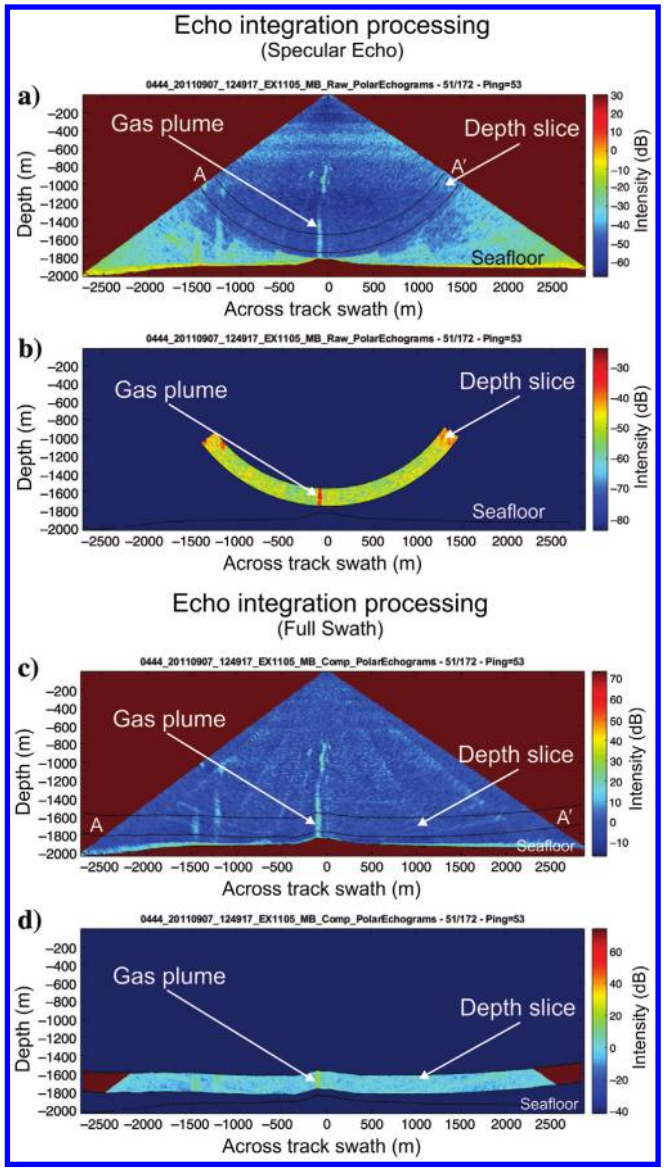

Figure 8. SonarScope EI workflow. (a) EI of the midwater within the specular main lobe at 85%–96% of water depth delineated by the black lines from profile A-A′ of a ping containing a plume anomaly. The lower image shows the extracted part of the echogram that will be vertically integrated to create the 2D backscatter raster shown in Figure 9a. (b) EI of samples integrated above the entire swath within the depth slice delineated by the black lines.

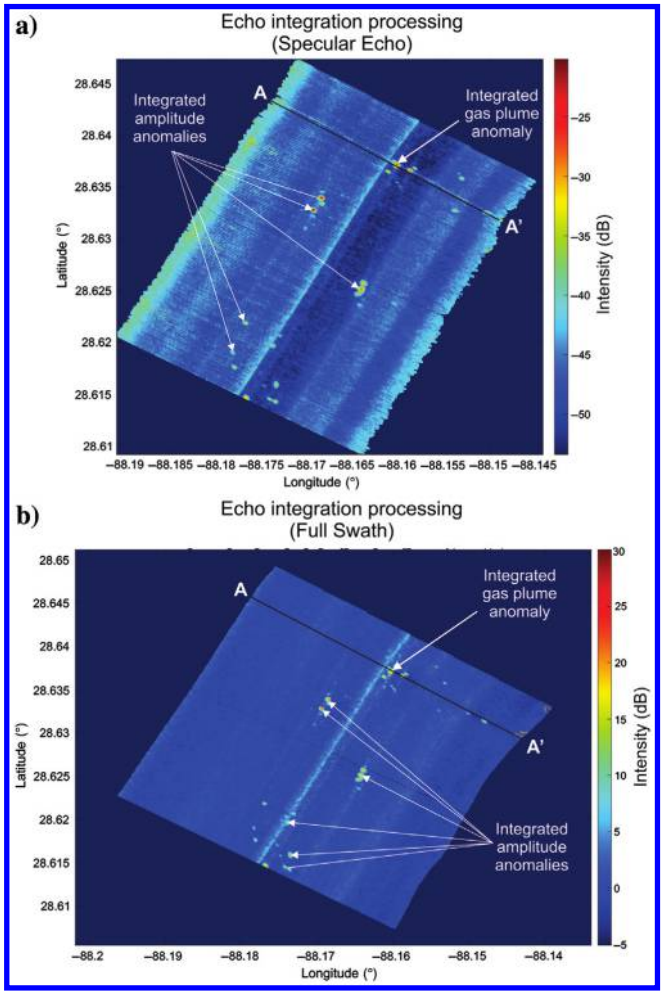

Figure 9. Mosaic results of EI in SonarScope for (a) the main specular echo and (b) whole swath. Profile A-A′ refers to the depth slice from Figure 8. Final backscatter mosaics were created using the whole swath width for greater seafloor coverage and clipped at a 55° swath angle to delete attenuation artifacts within the outer beams.

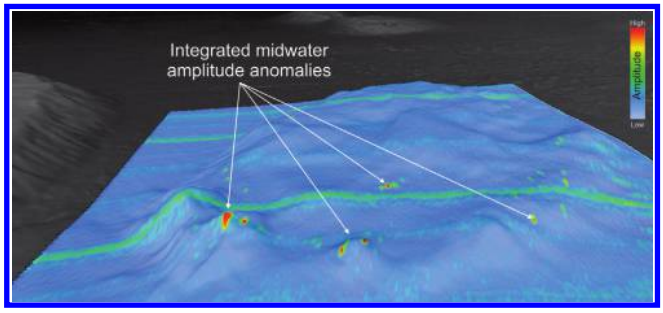

Figure 10. Visualization of the workflow from Figures 8 and 9 of EI from a MBES data example using 5 m Kongsberg EM302 multibeam data (NOAA EX1105) over Dauphin Dome in MC, GOM (VE = 3x). Draping results of echo integrated raster surfaces can be a powerful interpretive tool to delineate seafloor gas emission accurately.

NOAA exploration cruise EX1402L2 in the Gulf of Mexico

The Northern Gulf of Mexico (NGOM) features a complex seafloor morphed by active salt diapirism creating varied topography from relatively flat intraslope sedimentary basins to high-relief domes and ridges. This geologic framework promotes buoyant upwelling of hydrocarbon gases and fluids from the deep subsurface to the seafloor where seepage physically modifies the seafloor through precipitation of authigenic carbonates, sediment displacement via fluid expulsion, and supporting biodiverse chemosynthetic habitats (Fisher et al., 2007). Seeps develop near flanks of these salt domes where deep subsurface faulting has focused fluid flow in response to active salt tectonics creating various seep-related features such as pockmarks, mud volcanoes, and brine pools. Seismic studies of seafloor amplitude anomalies suggest that there may be up to 5000 geologically active seep sites in the NGOM where authigenic carbonate deposits have formed in response to upwelling hydrocarbons (Frye, 2008). Analyses into seafloor amplitude reflectivity maps suggest a prevalence and extensive geographic distribution of dense concentrations active deep (>500 m) hydrocarbon seeps (Roberts et al., 2006) in the NGOM. Hydrocarbon free gas of highly variable chemical composition is emitted as bubble plumes from focused vents within most of these larger active hydrocarbon seep sites. The bubble plumes are visible throughout the water column on acoustic data, and the bubbles are commonly coated with a thin layer of oil or methane hydrate coating (Leifer and MacDonald, 2003).

Exploring and characterizing the seafloor and associated benthic ecosystems of the NGOM has been a focus of the National Oceanic and Atmospheric Administration's (NOAA) Office of Ocean Exploration over the past few decades. In 2014, NOAA's Ship *Okeanos Explorer* conducted exploration mapping operations (Cruise EX1402L2, March to April 2014) more than 17,000 km^2 of unmapped seafloor southwest of Flower Garden Banks National Marine Sanctuary in the northwestern GOM (Figure 7). MBES data collected on this cruise focused on ecological connections between midwater and deepwater benthic habitats in water depths ranging from 500 to 1500 m over salt-influenced seafloor. During mapping operations in the

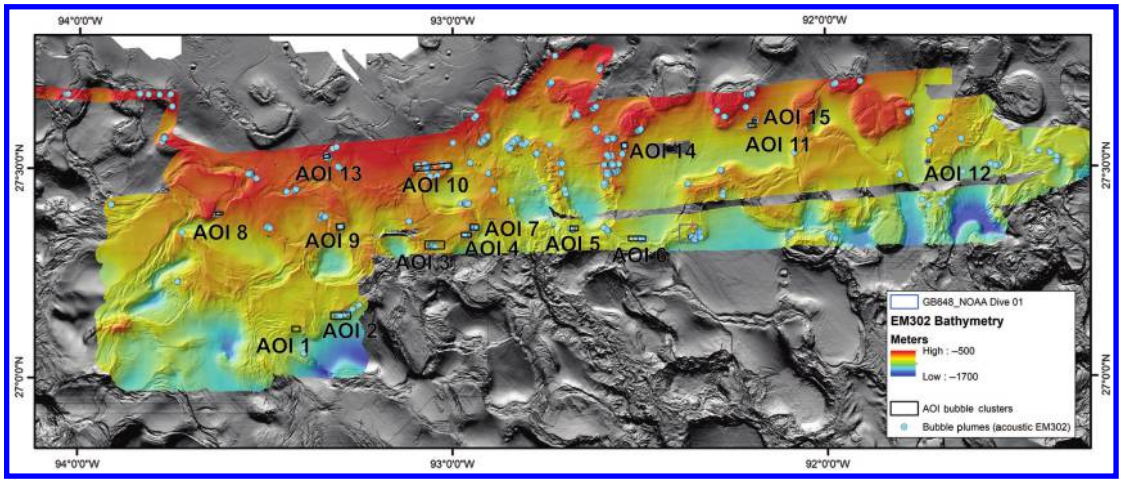

Figure 11. Bathymetric map of EX1402L2 showing locations of the 15 AOI over plume clusters.

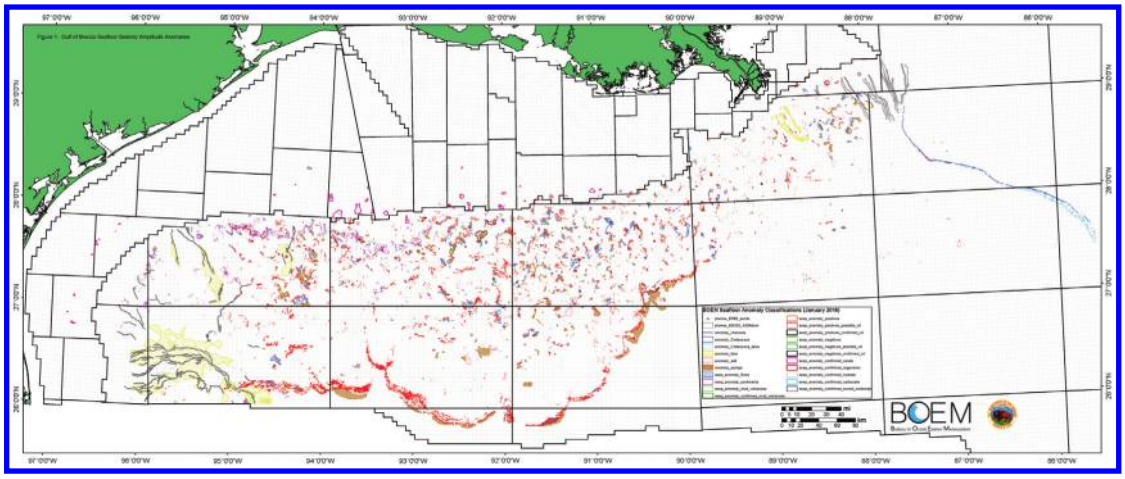

Figure 12. The GOM seafloor seismic amplitude anomalies in vector format provided by BOEM.

area, 695 water column anomalies were manually detected with a 30 kHz Kongsberg EM302 and interpreted by offshore NOAA physical scientists (McKenna, 2014) using FMMidwater. A primary science objective of EX1402L2 was to identify seeps and/or gas bubble plumes associated with benthic fauna and location of these water column anomalies were published in the final mapping report, included in the Bureau of Ocean Energy Management (BOEM) water-column gas plumes class contained in BOEM seafloor anomalies layer package and provided with the National Centers for Environmental Information (NCEI) data set. Therefore, these points are useful to evaluate variation of plume mapping uncertainty between a qualitative and quantitative seep mapping approach.

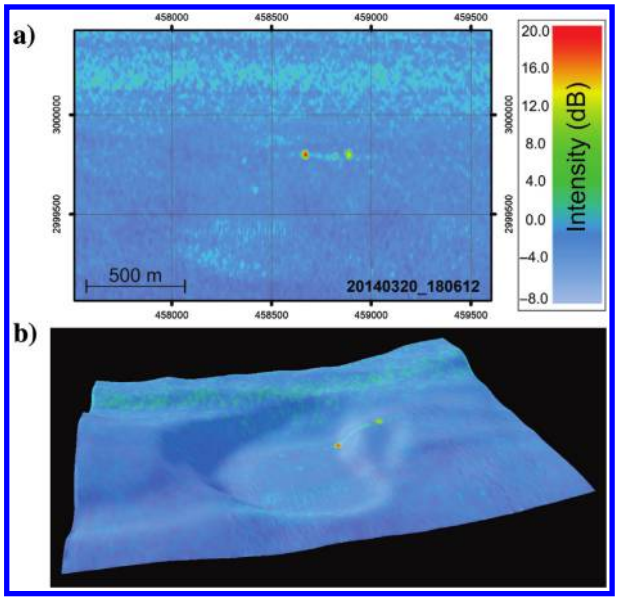

Figure 13. Two discrete point source plumes (+18 and +13 dB) located on peripheral of 500 m seafloor depression in area of high seafloor backscatter and amplitude in the multibeam and seismic data sets in (a) planar view and (b) perspective view. Water depth at approximately 960 m. The BOEM Seismic Water Bottom Anomalies Map features polygons in this area as seep_anomaly_positives and seep_anomaly_flows.

Comparison of mapping approaches

This study is designed to assess mapping uncertainty and confidence involved with the currently used midwater seep mapping techniques and to evaluate whether a vertical integration approach can improve the detection of seafloor venting of seep bubble plumes and their spatial distribution over large areas of seafloor. Multibeam data collected during the 2014 exploratory mapping cruise onboard the NOAA Ship *Okeanos Explorer* were used to create a 2D midwater backscatter mosaic. The resulting midwater amplitude mosaic is used as a baseline backscatter surface to evaluate accuracy of manual geopicks interpreted by NOAA physical scientists during the survey. An underlying assumption of this study is that discrete integrated high amplitudes in 2D midwater mosaics represent gas emission on the seafloor surface when these amplitude anomalies represent midwater samples between 85% and 96% of water depth. Within the scope of this study, we do not account for potential lateral offsets created by deepwater currents below and within the depth slice used. Figure 6 shows plume point clouds extracted by Feature Detector toolkit in FMMidwater (Gee et al., 2014) and their relationship with 2D vertically integrated midwater samples. In addition, a ground truthing example using remotely operated vehicle (ROV) dives (NOAA EX1402L3) and in situ observations of bubble emission are provided in the "Discussion" section to show natural ephemerality of gas release and mapping error.

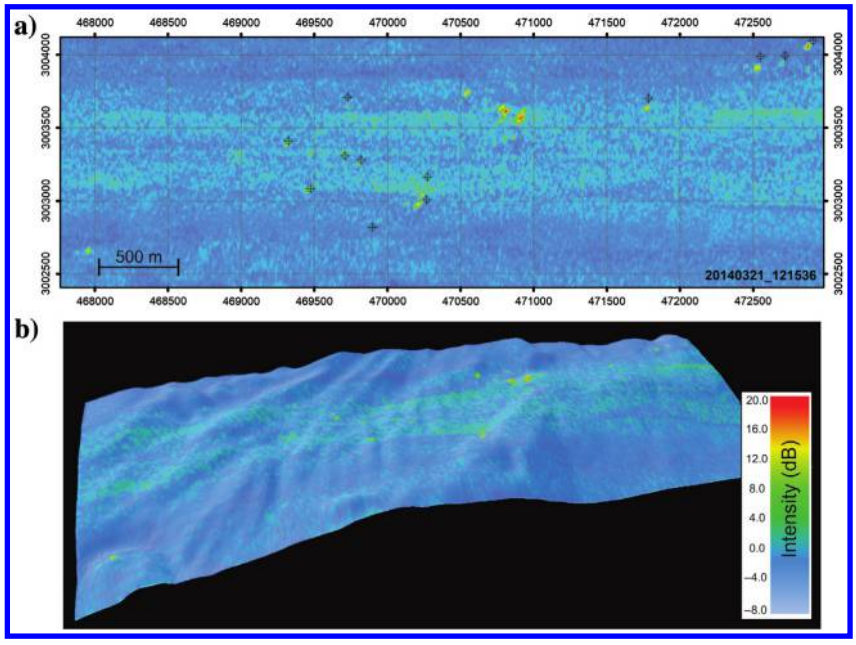

Figure 14. Plumes clustered along a faulted ridge crest with dB anomalies ranging +10 to +16 dB. This example highlights the general inconsistency of geopicking (black circled plus points) where offsets between an amplitude anomaly and geopick vary considerably. A high amplitude plume cluster subset in the center of the raster was missed by offshore interpreters. The BOEM Seismic Water Bottom Anomalies Map features polygons in this area as seep_anomaly_positives_possible_oil.

DOI:10.1190/INT-2021-0084.1

DOI:10.1190/INT-2021-0084.1

Methods

Data sets and processing

Raw MBES data were acquired from NOAA's Bathymetry Data Viewer hosted by NCEI in Boulder, CO. NCEI has archived water column sonar data sets since 2011, compiling submissions from NOAA and other academic vessels (Wall, 2016; Wall et al., 2016). Multibeam data acquired from NCEI consisted of raw Kongsberg *.all/*.wcd file pairs (145 GB for EX1402L2) along with cruise reports and locations of all observed bubble plumes in shapefile format. Processed bathymetry for each survey was downloaded from NCEI and viewed in context with the regional BOEM Deepwater Bathymetry layer (Kramer and Shedd, 2017) and the Seismic Water Bottom Anomalies layer package that delineates areas of acoustic anomalies associated with hydrocarbon seeps and carbonate hardgrounds (Roberts et al., 2006). MBES water column data were processed using SonarScope software (SonarScope-R2017b-64Bits-2019-07-02). Prior to EI processing, each data pair (*.all/*.wcd) was imported and inspected with QPS Qimera software to remove bad files and shallow transit data. Mosaics of echo integrated water column data were created using the angles and ranges algorithm with a 1-ping subsampling to create a series of raw and compensated polar echogram 32 bit tiff files for each ping, displayed in {Depth,AcrossDist} geometry with a −64 to +10 dB contrast stretch. The SonarScope workflow is shown in Figure 8. After each ping was converted into a polar echogram tiff file, the amplitude samples from 85% to 96% of the water depth (default parameter) were integrated for the main specular lobe (Figure 8a and 8b) and over the entire swath width (Figure 8c and 8d) for each *.all/*.wcd file pair creating two intermediate echo integrated data sets. Each mosaic of vertical EI was limited to a −55°/55° swath angle to account for attenuation effects in the far outer beams. Final mosaics were then generated using the complete swath width for increased data coverage

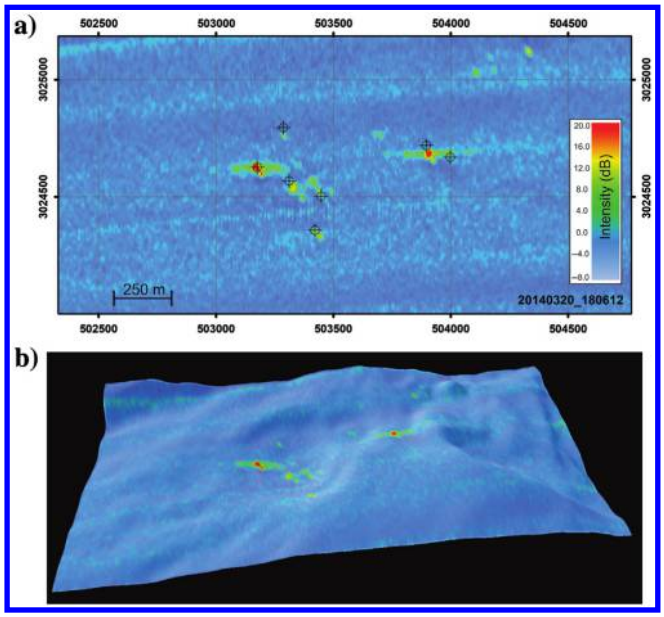

Figure 16. The AOI 4 features a cluster of very high amplitude point source plumes (20+ dB) that were detected by offshore interpreters in a shallow (20 m deep) seafloor depression. Several off-nadir plumes with moderate amplitude (+10 to 15 dB) were missed. The BOEM Seismic Water Bottom Anomalies Map features polygons in this area as seep_anomaly_positives.

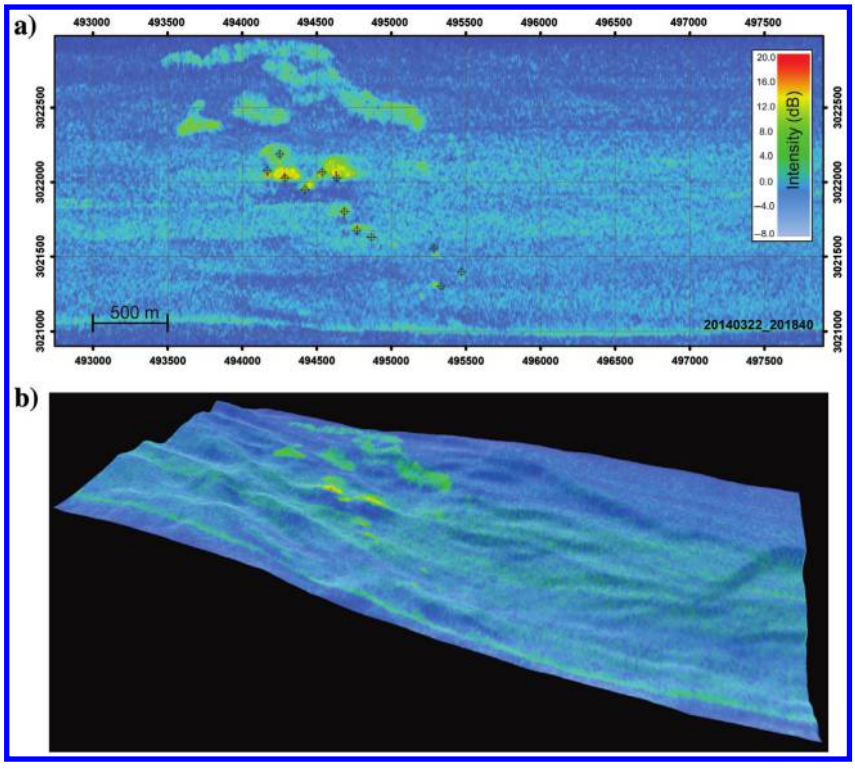

Figure 15. Prominent cluster of high amplitude water column anomalies with an unusual signature situated in area of seafloor faulting. Smaller point sources (+16 to 20 dB) located near diffuse area of moderate midwater backscatter that ranges from +3 to +8 dB. This signature could be due to significant bottom current or represent a specific form of fluid seepage than is observed in other areas. The BOEM Seismic Water Bottom Anomalies Map features polygons in this area as a water-column gas plumes class seep_anomaly_positives_confirmed_gas. Manual geopicks in this seep cluster detected areas of bottom emission accurately (0.5% of water depth).

using a limited number of successive MBES files (5–15 lines). This was to preserve the temporal aspect of these data within the mosaics; several lines had areas of overlapping coverage providing a measure of spatio-temporal variability of plume locations on the seafloor using this technique. Final echo integrated water column reflectivity mosaics were gridded at 5 m bin size and exported as ArcAscii (*.asc) files projected into UTM15N from SonarScope (Figure 9). Each backscatter raster mosaic was initially analyzed in Global Mapper and ArcGIS to locate amplitude anomaly interpreted to be bubble plume clusters and draped over underlying bathymetry for enhanced analysis (Figure 10). These anomaly amplitude locations (+12 to +25 dB) were compared with the NOAA geopick shapefile to further refine areas of interest (AOI) where interpreted plumes overlapped (EI-derived anomalies and NOAA geopicks). Fifteen final AOI mosaics were made from these larger multiline mosaics, and the corresponding *.wcd file for each was analyzed in

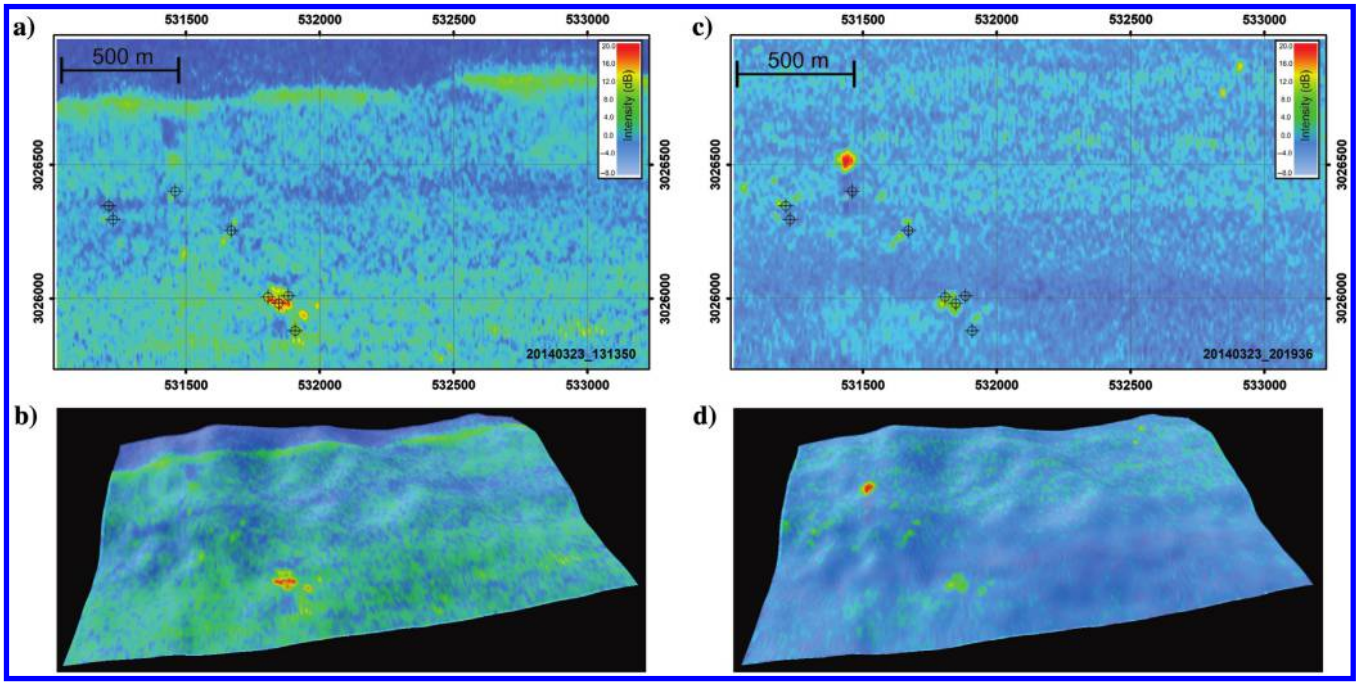

Figure 17. Time series example of a plume cluster in (a) planar and (b) perspective views with (c and d) the second pass approximately 7 h after the first pass. The first pass has a higher background noise level possibly due to weather, sea state, speed, and/or vessel heading. In the first pass, a main plume with an amplitude of +12 dB was detected accurately. In the second pass, this plume's target strength decreased to +8 dB. The bright high amplitude plume (+14 dB) seen in the second pass had increased the +4 dB seen initially providing a good example of how these plumes vary in strength and position over 7 h. The BOEM Seismic Water Bottom Anomalies Map features polygons in this area as seep_anomaly_positives_confirmed_gas.

Figure 18. Clusters of bright plumes located near faulting in GB 645 in 960 m water depth with amplitudes ranging from +10 to 12 dB. Several clusters were geopicked with accuracy and interpreters missed a dense group of +12 dB plumes in the west. The BOEM Seismic Water Bottom Anomalies Map features polygons in this area as a seep_anomaly_positives_confirmed_gas.

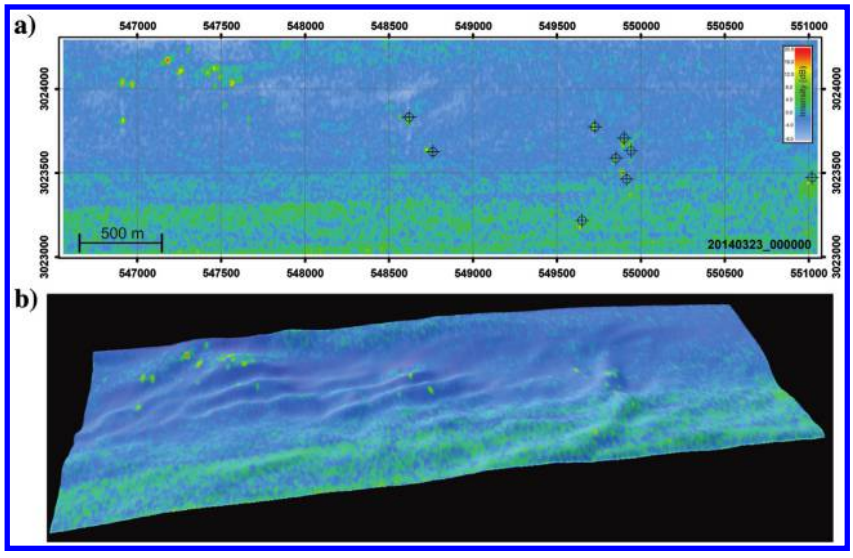

DOI:10.1190/INT-2021-0084.1

DOI:10.1190/INT-2021-0084.1

Table 1. Tabulated results of the EI mapping in each AOI with corresponding BOEM classifications.

			Seep-related anomalies				
	Results	BOEM Block	High-positive class	Low-positive/negative	Pockmarks class	Water-column gas plumes class	Appendix A Supplemental files (S1)
AOI 1	Figure 13	GB 846	seep_anomaly_positives, seep_anomaly_flows	—	—	—	Figure A-1, Figure A-2
AOI 2	Figure 14	GB 805	seep_anomaly_positives, seep_anomaly_positives_possible_oil	seep_anomaly_negatives_possible_oil	—	plumes_EM302_400ft_diam	Figure A-3, Figure A-4
AOI 3	Figure 15	GB 678	seep_anomaly_positives	—	—	seep_anomaly_high_positives_confirmed_gas, plumes_EM302_400ft_diam	Figure A-5
AOI 4	Figure 16	GB 636	seep_anomaly_positives	seep_anomaly_negatives	—	plumes_EM302_400ft_diam	Figure A-6
AOI 5	Figure 17	GB 642	seep_anomaly_positives	seep_anomaly_negatives	—	seep_ anomaly_high_positives_confirmed_gas, plumes_EM302_400ft_diam	Figure A-7, Figure A-8
AOI 6	Figure 18	GB 645	seep_anomaly_positives	—	—	seep_ anomaly_high_positives_confirmed_gas, plumes_EM302_400ft_diam	Figure A-9, Figure A-10
AOI 7	Figure 19	GB 636	seep_anomaly_positives	seep_anomaly_negatives	—	plumes_EM302_400ft_diam	—
AOI 8	Figure 20	GB 578	seep_anomaly_positives	—	—	—	Figure A-11, Figure A-12
AOI 9	Figure 21	GB 629	seep_anomaly_positives_possible_oil	—	—	—	Figure A-13, Figure A-14, Figure A-15
AOI 10	Figure 22	GB 645	seep_anomaly_positives_confirmed_oil	seep_anomaly_negatives_possible_oil	—	—	—
AOI 11	Figure 23	GC 648	seep_anomaly_flows, seep_anomaly_confirmed_organisms	seep_anomaly_confirmed_mud_volcanoes	—	—	—
AOI 12	Figure 24	GC 444	seep_anomaly_positives_possible_oil	—	—	—	Figure A-16
AOI 13	Figure 25	GB 452	seep_anomaly_positives, seep_anomaly_positives_possible_oil	—	seep_anomaly_pockmarks	—	—
AOI 14	Figure 26	GB 424	seep_anomaly_flows, seep_anomaly_confirmed_organisms	seep_anomaly_negatives	—	—	—
AOI 15	Figure 27	GB 388	seep_anomaly_confirmed_organisms	seep_anomaly_negatives	—	—	—

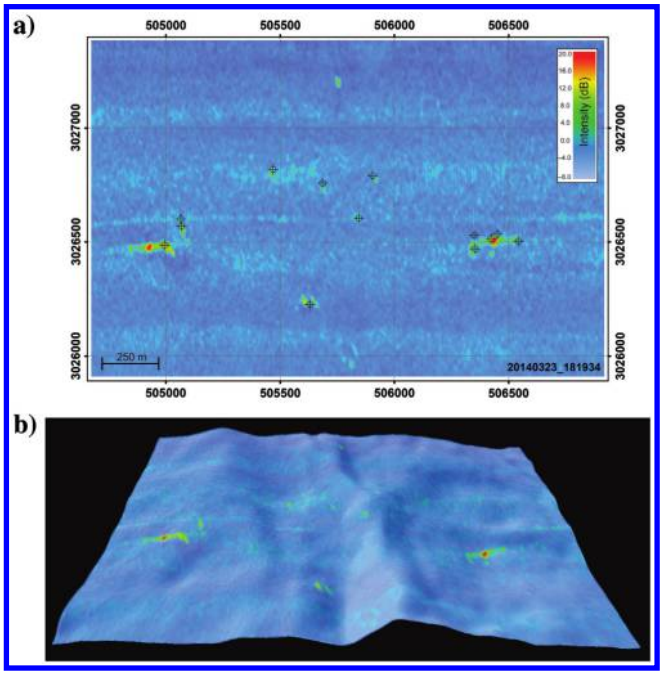

Figure 19. The AOI 7 shows two major point source bubble streams with amplitudes of 20+ dB. Smaller moderate amplitude plumes of +10 to 12 dB were detected accurately in FMMidwater with exception of single bubble site in the north. The relatively clean data observed in the main lobe drops off in quality significantly likely leading to the undetected off-nadir plume. The S/N of the backscatter mosaic is higher than the FMMidwater lateral stacking. This example shows consistent manual detection with exception of off-nadir outlier. The BOEM Seismic Water Bottom Anomalies Map features polygons in this area as seep_anomaly_positives.

FMMidwater using the default settings (i.e., Deep Mode fore/aft swaths and no downsampling). Each *.gwc file was viewed in side stack with data quality noted before each ping was viewed in single ping mode (with geopicking functionality) and 10 ping lateral stack view.

Data analysis and visualization

Raster mosaics of each of the 15 AOI areas were viewed in ArcGIS (v. 10.7.1) and QPS Fledermaus (v. 7.8.11) software. In ArcGIS, geotiffs of the backscatter mosaics were created using hillshaded bathymetry (gridded at 20 m) at 50% transparency transposed over the colocated midwater backscatter raster to show geophysical context of the underlying terrain (Figure 8). These geotiffs were imported into Fledermaus and texture mapped over bathymetry where a 3D perspective could be viewed alongside a planar ArcGIS map. Color map for the EI results used the midwater.cmap range (clipped to −8 to +20 dB) provided in Fledermaus. To examine the spatial relationship midwater plume anomalies with high seafloor reflectivity, *.all files from each AOI were processed in Fledermaus Geocoder (FMGT v. 7.9.5) with a 5 m grid and viewed in standard deviation.

Once final maps were made in 2D and 3D perspectives, plume anomalies in the EI backscatter rasters were measured against the provided plume geopicks noting if a plume was missed (verified in FMMidwater), average offsets, data quality, and target strength of plumes in the EI rasters. For purposes of this study, accurate geopicks are defined to be within a range of

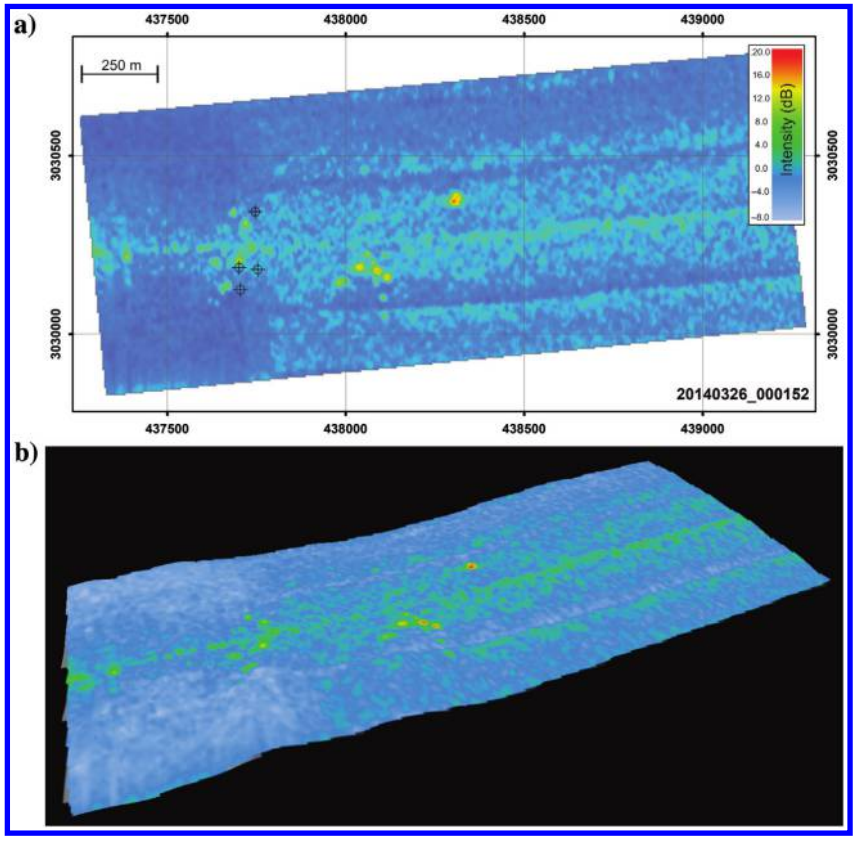

Figure 20. Very poor data quality due to weather along this section led to some masking of major plumes in FMMidwater. S/N is significantly heightened in the EI example although some acoustic noise is still present. The BOEM Seismic Water Bottom Anomalies Map features polygons in this area as seep_anomaly_positives.

DOI:10.1190/INT-2021-0084.1

0.5% water depth from the midwater anomaly (precision of USBL-navigated coring).

Results

Geovisualization atlas of bubble plumes in the EX1402L2 study area

EI results of EX1402L2 multibeam midwater data over selected sites highlighting disparities in the digitizing technique are listed in Table 1 with supporting geovisualizations shown in Appendix A, which can be downloaded as a supplemental file (S1). Each of the selected 15 AOI contained acoustic anomalies indicative of bubble plume clusters that were identified in the midwater backscatter mosaics and confirmed in beam fan view within FMMidwater software. Locations of the selected AOI are shown in Figure 11. Each AOI shows a 2D midwater backscatter mosaic (projected into UTM15N) and the location of the NOAA interpreted geopicks (black circled plus points) along with a 3D Fledermaus perspective (vertical exaggeration = 3x) rendering for bathymetric context. Each image is time-stamped and includes the BOEM amplitude anomaly classification(s) found in each AOI for geologic and seep-related context. Appendix A, which can be downloaded as a supplemental file (S1), contains geovisualizations of bathymetry and seafloor backscatter for geologic context along with FMMidwater examples for insight into midwater data quality, which can impair manual interpretation.

BOEM Seismic Water Bottom Anomalies Classification GIS layer

Each of the 2D midwater mosaics was viewed in context of the available Seismic Water Bottom Anomalies Classification GIS layer. This layer package (v. June 2019) contains vector polygons (approximately 37,000) related to the distribution of natural hydrocarbon seeps and related benthic fauna (chemosynthetic and coral communities) in the GOM based on the mapping and interpretation of seafloor acoustic amplitude from 3D seismic surveys and verified anomalies from submersible, remotely operated vehicles (ROVs), autonomous underwater vehicles (AUVs), camera sled surveys, piston cores, trawls, and multibeam sonar identifying water column gas plumes (Figure 12). BOEM denotes four major classes of anomalies related to hydrocarbon seepage — high-positive, low-positive/negative, pockmarks, and a water-column gas plumes class. A high-positive class is the most common in the data set, often showing hydrocarbon migration pathways on vertical seismic profiles and exhibiting a slow to moderate rate of hydrocarbon seepage. A low-positive class has an acoustically slower response than of typical hemipelagic mud of the GOM. The pockmark class denotes areas interpreted to be created by the removal of sediment through rapid gas expulsion. The water-column gas plumes class represents detected gas plumes from the *Okeanos Explorer's* Kongsberg EM302 MBES acquired during 2011, 2012, and 2014 surveys with a 400 ft diameter of uncertainty. Table 2 contains descriptions of these various BOEM classes. AOI plume clusters 1–15 are shown in Figures 13, 14, 15, 16, 17, 18, 19, 20, 21, 22, 23, 24, 25, 26, and 27, respectively.

Discussion

Accuracy of manual geopicks

Mapping comparisons between the traditional manual digitizing of plumes in FMMidwater beam fan view versus a 2D integrated midwater amplitude raster show varied positional uncertainty. There is a general discrepancy in accuracy between these digitized geopicks and the amplitude anomalies in the midwater backscatter maps. Several examples show fairly accurate (within 0.5%–1% of water depth) (AOI 4 and 12), to larger offsets of 60–100 m (AOI 10 and 15), to larger missed plumes of high amplitude (20+ dB). Many were located on the same line where there was a series of accurate detections, followed by areas of undetected high-amplitude plumes,

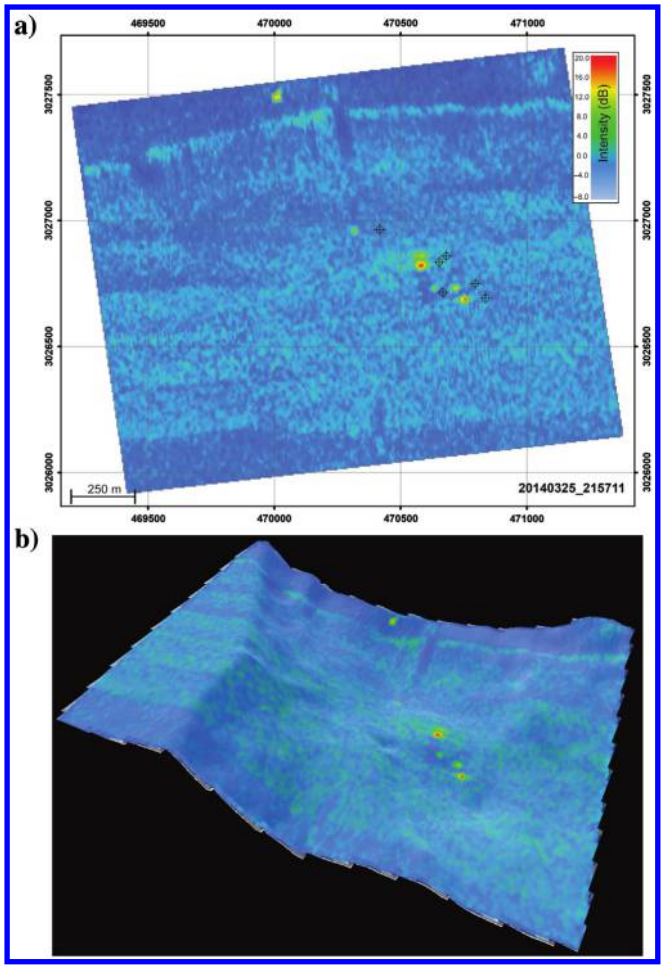

Figure 21. A data example like AOI 8. This is a weather-degraded line with overall high elevated background noise. Offset manual geopicks are 80–100 m from emission sites of 18–19 dB. A large undetected plume of moderate target strength located in the north. The BOEM Seismic Water Bottom Anomalies Map features polygons in this area as seep_anomaly_positives_possible_oil.

DOI:10.1190/INT-2021-0084.1

and followed with more accurate digitizing (AOI 2, 6, and 11). Concerningly, from a commercial seep hunting standpoint, several plumes that were manually digitized appeared to be either environmental or system noise (AOI 2, 10, and 13).

Science objectives for this cruise included identifying benthic habitats in the area using gas plume location as a proxy for estimating the seafloor distribution of chemosynthetic communities. Therefore, it is safe to assume that the NOAA physical scientists on watch were actively scrutinizing the midwater data for plume anomalies. NOAA reporting for EX1402L2 (McKenna, 2014) note "bubble plumes that were observed and noted in real time by watch-standers using the data acquisition software helped detect bubble plumes during post-processing analysis of the water column backscatter in QPS. 'Fan view' and 'Stacked view' were used in the QPS water column tool to identify possible bubble plumes. The locations of the bubble plumes detected in each line were then exported into a text file."

Each of the 15 AOIs used were inspected in FMMidwater to attempt to speculate on why these plumes may have been missed or inaccurately mapped. A common cause for the large offsets seen is due to geopicking higher up in the water column where the plume may have a cleaner signal that is easily identifiable. Usually overlooked, this technique can translate into a sizeable lateral offset on the seafloor. Using a second window within FMMidwater displaying a stacked ping window

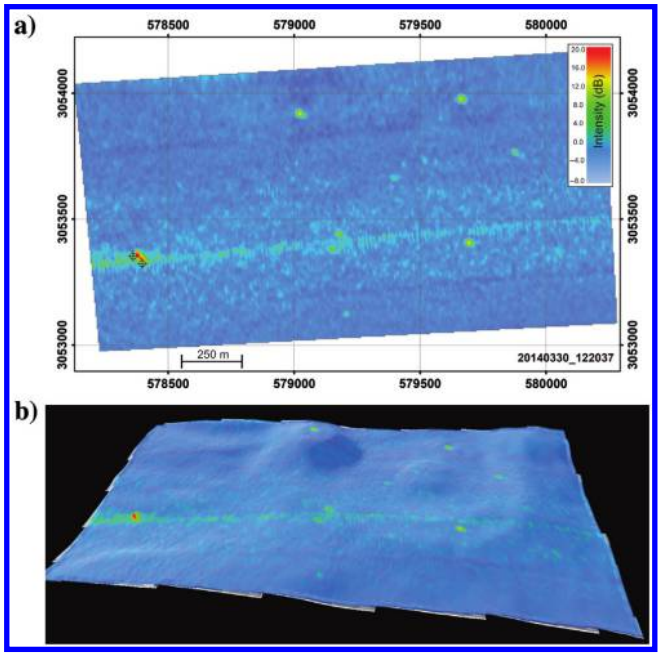

Figure 23. Very accurate geopicking on a high amplitude (20+ dB) near-nadir plume anomaly. Multiple discrete plumes of moderate amplitude (+10 to 12 dB), near and off nadir were missed on top of BOEM classified seep_anomaly_confirmed_mud_volcanoes and seep_anomaly_confirmed_organisms. A seep_anomaly_flows polygon is located adjacent to the site.

Figure 22. Large cluster located in BOEM-designated seep_anomaly_positives_confirmed_oil anomaly polygons. Relatively poor manual detection of oil plumes near nadir. In general, oil plumes have high amplitude signatures — many of the brightest plumes in this area were 20+ dB. Manual offsets ranged from 60 to 100 m from plume emission site.

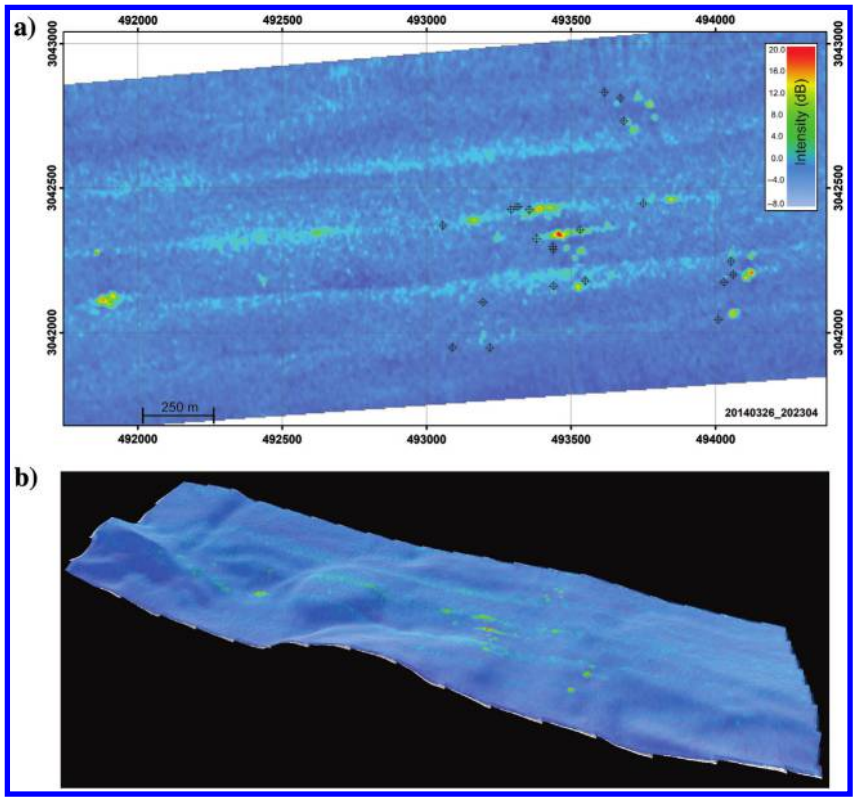

DOI:10.1190/INT-2021-0084.1

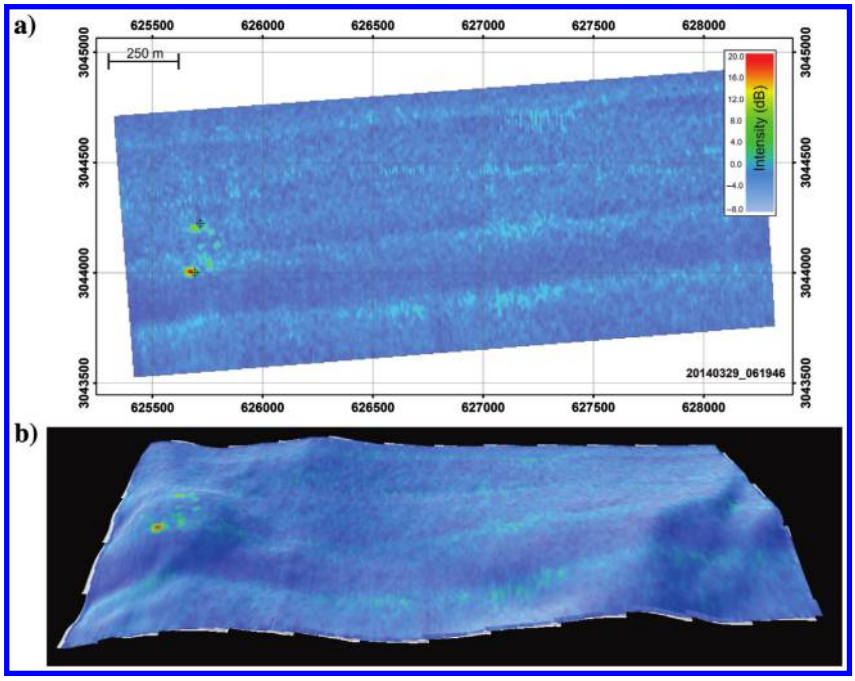

Figure 24. The AOI 12 features a discrete and high amplitude (20 dB) plume detected accurately in clean midwater data. Several smaller plumes of 10–12 dB found in area. The BOEM Seismic Water Bottom Anomalies Map features polygons describe this area as seep_anomaly_positives_possible_oil.

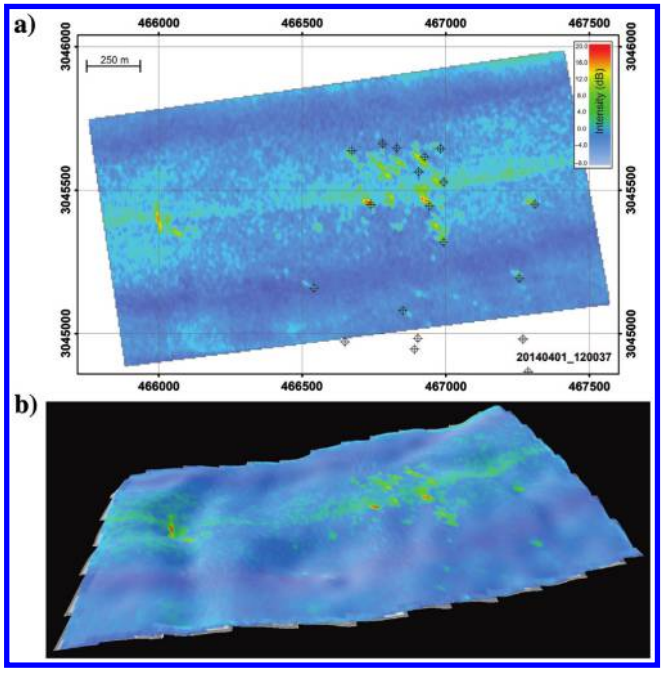

Figure 25. Large plume cluster with main plumes of 18 dB located near moderate strength (12 dB) plumes with linear signature. This could potentially represent strong bottom currents pushing vertically ascending bubbles laterally over seabed. The large plume in was undetected by the author using FMMidwater. The BOEM Seismic Water Bottom Anomalies Map features polygons in this area as seep_anomaly_positives_possible_oil.

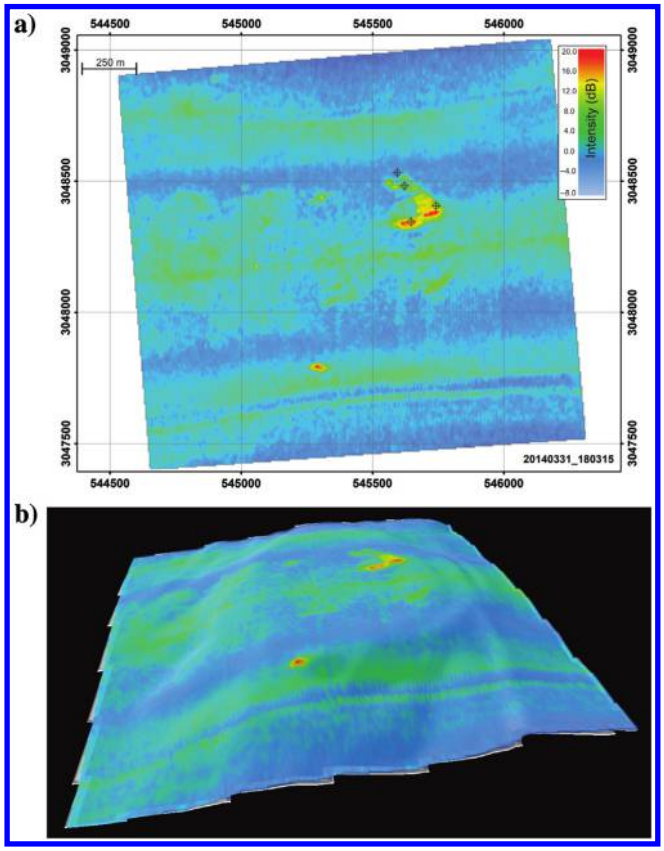

Figure 26. Accurate geopick on plume cluster (18 dB) on a plateau of an expulsion feature but missed high amplitude (18 dB) plume along flank of feature. The BOEM Seismic Water Bottom Anomalies Map features polygons in this area as seep_anomaly_confirmed_organisms, seep_anomaly_negatives, and seep_anomaly_flows.

DOI:10.1190/INT-2021-0084.1

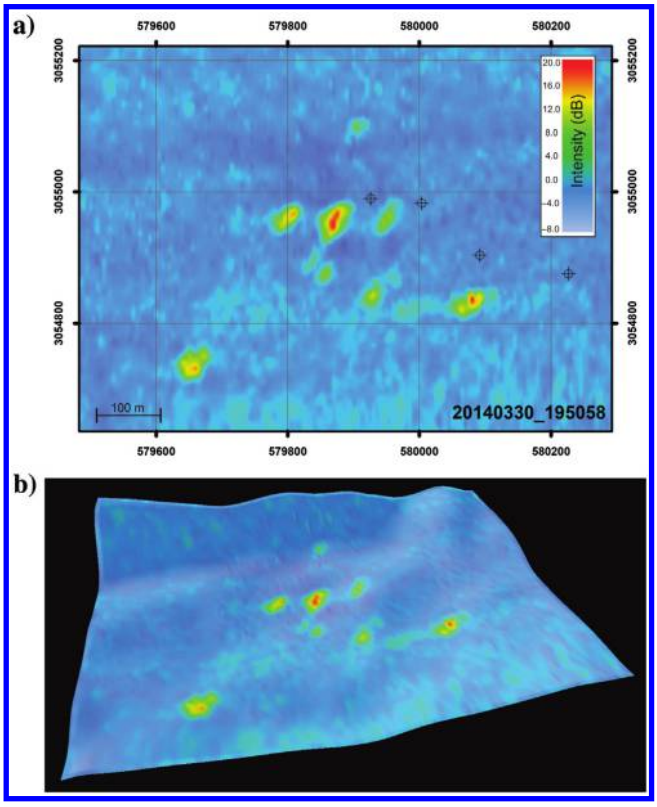

Figure 27. The AOI 15 showing general poor manual detection of otherwise bright, high amplitude plumes (17 dB). Geopicks displayed offsets 80–100 m from base of plumes possibly from off-nadir location of plumes. Offsets could be due from manually digitizing the plume high up in water column. This AOI is near AOI 11 and features BOEM characterized seafloor of seep_anomaly_confirmed_organisms located in the center of a seep_anomaly_negatives polygon.

(10–15 pings) can help improve the S/N is successive images to locate plumes. Several examples showed almost undetectable plumes with faint target strengths (<10 dB) in the single ping window that were clearly visible in a lateral stacked view. Not using this stacked window during manual interpretation would contribute to missed plumes. However, lateral stacking greatly exacerbates background noise and plumes found outside of the main lobe region can be masked by the artifacts (Figure 28). Survey EX1042L2 was conducted in March 2014 and sea state along with typical *Okeanos Explorer* survey speeds of 8 kts regardless of water depth can contribute to data quality degradation. Poor sea state was noted in the data log from 24 to 30 March, where surveyors adjusted the forward tilt of the sonar head. This improved bathymetry data at the expense of the seafloor backscatter data quality. Acquisition settings to obtain high-quality seafloor backscatter usually translate to high-quality midwater backscatter. Several FMMidwater examples showed such examples of degraded midwater data in the outer beams outside of the main specular beam region. Vertically stacking midwater data produced a measurably higher S/N than lateral stacking pings showing that the EI mapping can be used to help detect plumes even in marginal noisy sea states. Figure 28 shows the difference between lateral stacking and vertical stacking quality differences. It is significantly easier to locate the exact position of the highest amplitude in the vertical stacked data (inset map).

During FMMidwater confirmation of plumes seen in EI AOI raster surfaces, the author notes the exhaustive time spent viewing each data line on a ping-by-ping view. Manually geopicking was difficult on most lines with

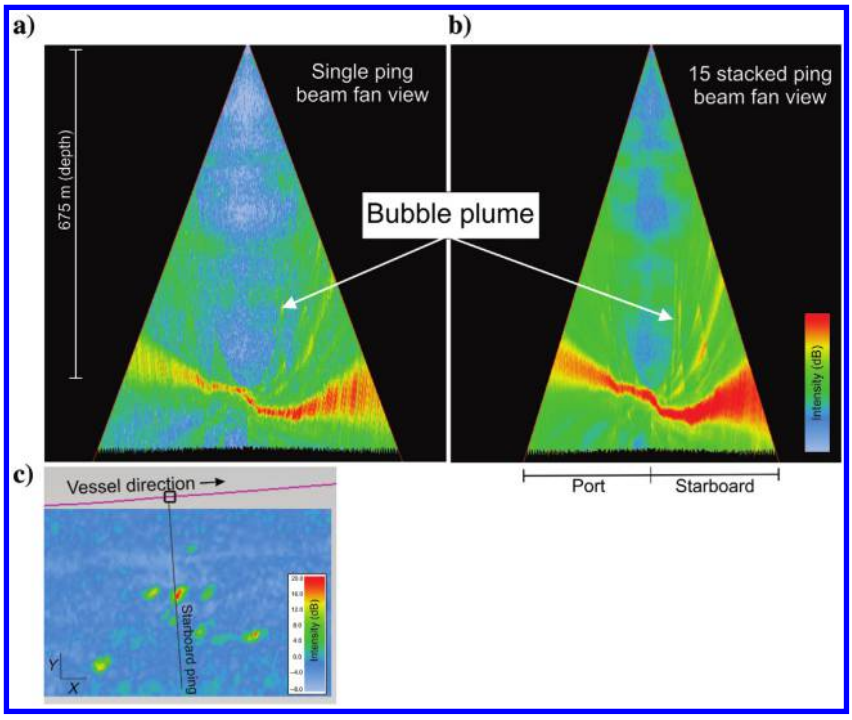

Figure 28. Data example of AOI 15 in FMMidwater. This line was collected in a marginal sea state and plumes in this area had a substantial lateral offset from the midwater backscatter amplitude maps. Note the clean data quality in the EI inset map that clearly shows the high amplitude plumes. These are hard to discern in the (a) single ping view except for high up in the water column. Slight deviation in the plume's vertical ascent can contribute to these 100 m offsets. Viewing the data in the (b) stacked ping view shows the plume cluster at a slightly higher amplitude than the integrated background noise making it difficult to discern the gas source near the seafloor. (c) Plan view of vessel orientation with underlying EI backscatter grid for reference.

offsets up to 100 m, whereas several were more accurate. Several large high amplitude plumes were missed in this slow and tedious manual inspection. On lines that were inspected multiple times, the author was unable to repeat mapping many geopicks showing how this process is subjective, prone to user fatigue and focus, and monotonous. Viewing the same data processed into a vertically stacked product takes less than a minute.

Figure 29 shows hypothetical range rings of 35 m radii from the geopicks over this plume cluster in 700 m depth. During commercial seep surveys, core targets can be precisely sampled using USBL assisted navigation technology to 0.5% of water depth. If these geopicked points were used as sole core target criteria, would a chemical signal indicative of hydrocarbon seepage be detectable? It shows why these points need to be carefully interpreted in context with underlying seafloor reflectivity and bathymetry for successful seep surveys.

For commercial seep hunting practices, we are interpreting water column data incorrectly. Although geopicking has been common practice since the adoption of midwater mapping technology into seep hunting, it was initially intended for use as a hydrographic tool. In 2014, QPS released a Feature Detection/Seep Hunter toolkit within FMMidwater allowing a user to extract water column anomalies be quantitatively extracted from the data using threshold filtering and other automated procedures (Gee et al., 2014). This toolkit uses iterations of normalization and despeckle algorithms to isolate points of interest, which are then exported as xyz(a) points. Further cluster analyses can be performed on the resulting 3D point cloud to remove high amplitude outlier points. This tool was adopted into the Fugro Seep Group for the TGS *Gigante* and *Otos* seep surveys, and it was used primarily in our workflow as a postsurvey and analytical tool for data visualization. This tool is currently being used to explore the relationships between 3D plume morphology and geochemistry (can a differentiation be made using MBES water column imaging between oil droplets versus pure methane gas versus methane hydrated coated bubbles?). Although this tool is very powerful for creating 3D plume models, it lacks the fully automated potential of creating a raster product that can be viewed in a GIS as a data reconnaissance tool for seafloor interpretation.

Gee et al. (2014) conduct a similar study to assess plume detection uncertainty between geopicking and the feature detection module using the EX1402L2 data set. They note that the original processing of 300 lines of water column data offshore was conducted in more than 40 h interpreting the (695) plumes via manual digitizing. A subset of the data set (10% of survey lines) was reprocessed manually onshore to evaluate differences between two interpreters. They found that the strong scattering plumes near nadir were consistently detected by both interpreters where weaker seeps in the outer beams were only detected approximately 50% of the time. To evaluate the manual detection results with

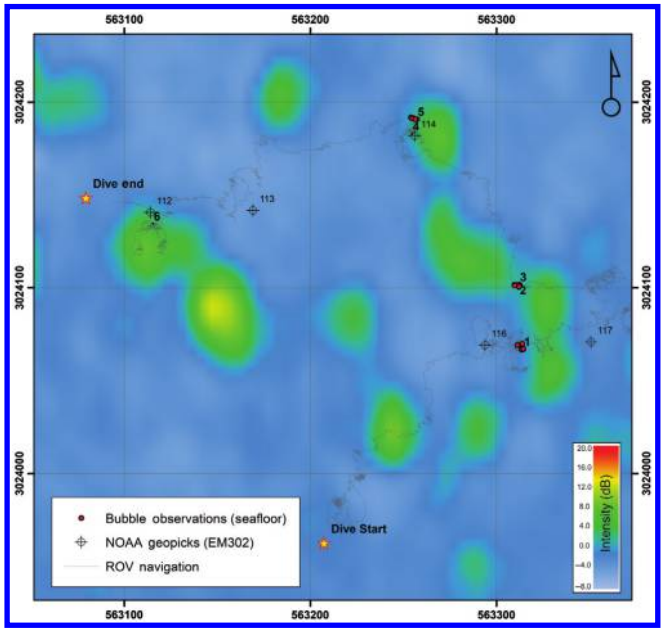

Figure 30. The EI results over GB 648, the site for NOAA ROV Dive 01 on EX1402L3. All dive observations mentioning bubble streams from the ROV dive log are in red points. Numbered areas represent image locations in Figure 31. Figure 31a = 1, Figure 31b = 2, Figure 31c = 3, Figure 31 d = 4, Figure 31e = 5, and Figure 31f = 6.

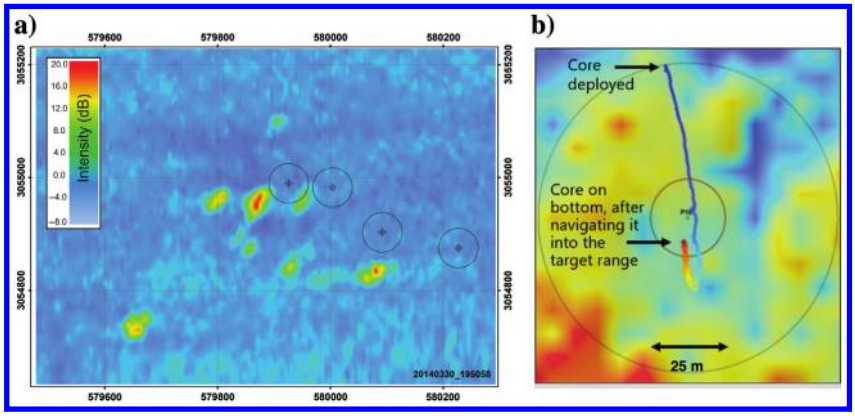

Figure 29. (a) The 2D raster of EI backscatter data from AOI 15 showing 35 m range rings that hypothetically represent USBL core position uncertainty (0.5% of 700 m water depth). If these geopicks were used as coring locations (in the absence of other geophysical data sets), would a geochemical signal be detected? (b) An example of USBL-guided core positioning to sample within the target area.

DOI:10.1190/INT-2021-0084.1

the module, this subset of water column lines was processed using default settings. The results showed that this semiautomated detection module located most of manual geopicks with a few false positives. A useful future uncertainty study could compare the EI method with their 2014 automated results to analyze where the discrepancies lay between two quantitative mapping techniques.

During EX1402L3, the third and final leg of the 2014 GOM expedition, 16 telepresence-enabled ROV dives were conducted over priority areas based on previously acquired mapping data. Two of these dives were on cold seep sites, with one of these (Dive 01 EX1402L3 at GB 648) located within the EX1402L2 survey area (Figure 11). ROV dives provide a way to ground truth these mapping results from this study using in situ camera imagery of active seeps. The purpose of Dive 01 at GB 648 was twofold — (1) assess if high seafloor backscatter from the EM302 MBES and high seafloor reflectivity (3D seismic/industry data contained in the BOEM Seismic Water Bottom Anomalies Classification GIS layer) were associated with carbonate hardgrounds and (2) to ground truth the interpreted seafloor locations of the plume detection as discrete sites of gas venting.

Figure 30 shows vertically integrated midwater data from EX1402L2 with the location of the manual geopicks with ROV track lines. The ROV data log was used to obtain geographic positions of any near-seafloor descriptions of "bubbles." All imagery was reviewed, and images showing bubble characteristics and seep-related features were mapped. The ROV track appears to have used the manual geopicks as seafloor waypoints and located five discrete cold seeps with numerous bubble streams observed during the dive. There is a strong correlation to the high amplitude areas from the EM302 data set (acquired on 23 March 02:00) and the ROV Dive 01 (12 April 13:49 to 21:32). Figure 31 shows selected images from the dive where Figure 31a–31f is numbered (1–6) in Figure 30. Outcrops of hydrate (Figure 31a and 31d) were observed along with living buccinid mussels at the base of these hydrate covered outcrops. Bubbles with various geochemical makeup and characteristics were observed from oily brown (Figure 31b and 31c) to clear (Figure 31e). Other sites of gas venting feature gas bubbles encased in hydrate. This geochemical ground truthing can provide potential insight into specific geochemical signatures seen in midwater amplitude maps.

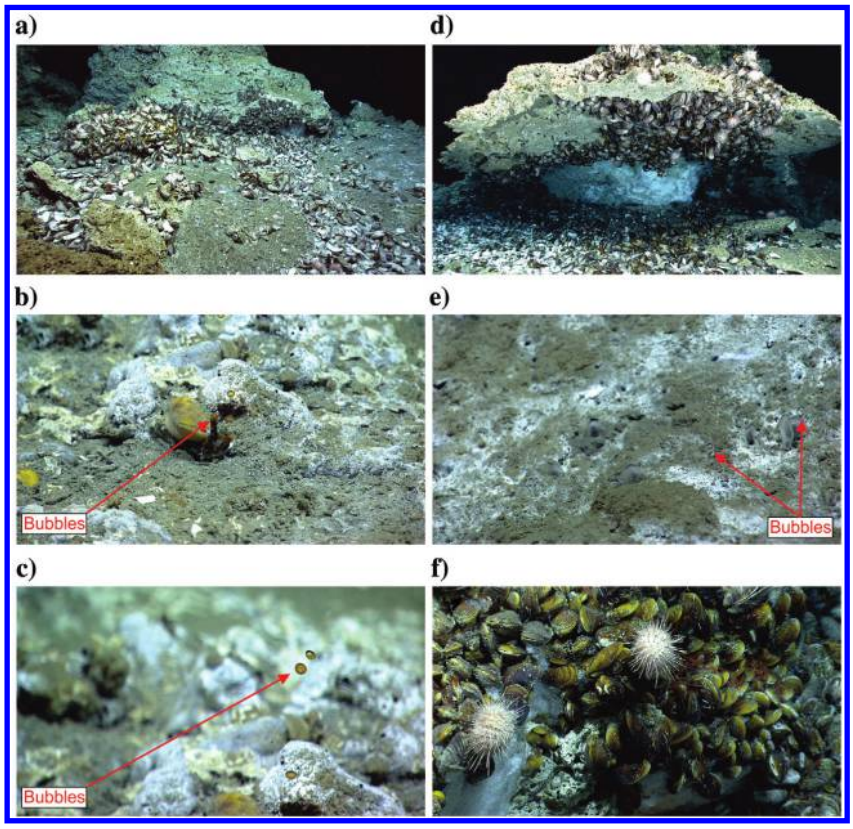

Figure 31. Seep-related images acquired during ROV Dive 01 at GB 648. First column are images (a-c), and second column are images (d-f). (e) Bubbles emitted at GB 648 exhibit varying chemical makeup from clear pure methane gas, (b and c) the oily brown "dirty" bubbles, and hydrate encased bubbles.

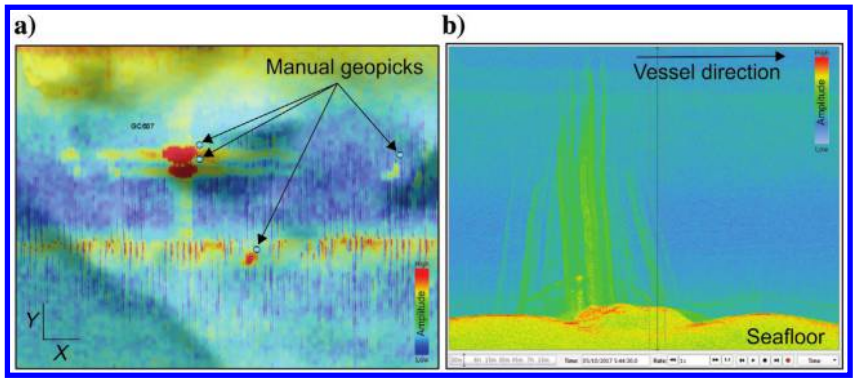

Figure 32. (a) The EI example of a "ghost" plume showing offset geopicks in 2D planar view. (b) A ghost plume shown in range stacked data view. When interpreting plume positions using a lateral stacking method, the true emission site can be masked by sensor artifacts.

DOI:10.1190/INT-2021-0084.1

Table 2. BOEM seep-related anomalies classification descriptions found within each AOI in the study.

		Class	AOI	Description
Seep-related anomalies	High-positive	seep_anomaly_positives	1,2,3,4,5, 6, 7, 8, and 13	High-positive amplitude anomalies that have not yet been confirmed as seep-site hardgrounds — they are purely seismic interpretations.
		seep_anomaly_confirmed_organisms	11, 14, and 15	High-positive amplitude anomalies that have been confirmed to be hardgrounds with predominantly chemosynthetic communities, although most have corals to a minor extent. Confirmed via manned submersibles, ROVs, AUVs, camera sleds, trawls, and piston cores either by academia, government, or industry sponsored cruises.
		seep_anomaly_positives_possible_oil	2, 9, 12, and 13	High-positive anomalies located directly below sea surface oil slicks, or within one water depth's distance. Although not directly observed to be seeping oil, we are calling these possible oil seeps due to their proximity to the slicks. They are likely to have chemosynthetic and coral communities living on the carbonate hardgrounds.
		seep_anomaly_positives_confirmed_oil	10	High-positive anomalies that have had direct observations of oil seepage from the seafloor by submersible, ROV, and/or analysis of piston cores, and all have had chemosynthetic and coral communities living on the carbonate hardgrounds.
		seep_anomaly_flows	1, 11, and 14	High-positive amplitude anomalies interpreted to be flows of sediment out of high flux vent sites on steep slopes. They either (1) contained hydrocarbons and were subsequently partially lithified, (2) attracted chemosynthetic clams which consumed what hydrocarbon was available (and because they were not located at the active seep site, subsequently died), or (3) are made up of acoustically faster sediment (i.e., sand). The flows that have been visited by submersibles often are a combination of two or more of the preceding.
	Low-positive/negative	seep_anomaly_negatives	4, 5,7, 14, and 15	Show an anomalously low-positive amplitude response on seismic compared with the typical hemipelagic muds. The most active and dynamic of this type exhibit a negative amplitude response, or acoustic trough, at the seafloor, resulting from a total phase reversal of the seafloor's typical positive acoustic impedance. These areas have been observed to have rapid hydrocarbon flux, often with sediment and brine being expelled with the hydrocarbons.
		seep_anomaly_confirmed_mud_volcanoes	11	Confirmed by direct observation. Just as with the high-positive anomalies, all negative anomalies were checked on the vertical 3D seismic profiles to confirm they are caused by a seep with active migration.
		seep_anomaly_negatives_possible_oil	2 and 10	Low-positive/negative anomalies that are either directly below sea-surface oil slicks or are within 1 water depth's distance, and therefore could be the source of the slick, but not yet confirmed to be.
	Pockmarks	seep_anomaly_pockmarks	13	Are circular to oval depressions interpreted to be created by the removal of sediment through rapid, and possibly, explosive gas expulsion. Few pockmarks have visible active migration pathways on vertical seismic profiles, but most appear to be dormant and without discernible active migration. Rapid expulsion is interpreted to be exclusively gas and appear to be purely destructive due to the removal of sediment. No sediment, brine, or oil expulsion has been observed during direct observations. Due to a lack of hard substrate and absence of continuing seepage at most pockmarks, chemosynthetic organisms and corals are unlikely to be associated with them.
	Water-column gas plumes	plumes_EM302_400ft_diam	2, 3, 4, 5, 6, and 7	400 ft diameter circles to indicate the uncertainty of the exact seep location on the seafloor, which varies with water depth. You will note many of the circles are clumped nearby each other. Due to the nature of overlapping swath data acquisition, some of those clumps may actually represent a single seep from the same spot on the seafloor; some are near the center of the swath (most accurate) and some well away from the center of the swath (less accurate). This is why there is a 400 ft diameter of uncertainty.
		seep_anomaly_high_positives_confirmed_gas	3, 5, and 6	High-positive anomalies that have either EK 60 and/or EM302 gas plumes identified to originate from within the anomaly polygon.

DOI:10.1190/INT-2021-0084.1

Advantages for echo integrating midwater backscatter data

EI offers several immediate advantages over the manual geopicking of hydrocarbon plumes. This methodology offers the ability to automate water column data processing where midwater amplitudes can be vertically stacked resulting in a quantitative perspective of the spatial distribution of hydrocarbon plumes on the seafloor. This method will allow for a percentage of water depth to be integrated and then displayed as a 2D amplitude map that can be imported in GIS software. This surface allows for rapid review of the entire data set where anomalies can be easily recognizable. This backscatter surface will provide an improved way to analyze plume emission areas and provide more valuable coring targets with higher mapping accuracy at a fraction of the time. There are four fundamental advantages associated with this approach within seep hunting — (1) efficiency of geoscientists offshore (more time can be spent on real-time monitoring of acquisition and interpretation than lengthy processing), (2) compression capability for remote survey services (a processed 2D ArcAscii (xya) midwater backscatter surface can zip to 1% of its original size and transmit ashore to the office and clients), (3) a 2D map of midwater backscatter amplitude over the survey area will provide greater accuracy of locating fluid venting sites, and (4) decreased project costs through automation.

Vertical stacking midwater data over lateral stacking techniques available in FMMidwater (side R-Stack or beam view stacked images) offers a visible improvement for interpreting a seafloor source of gas bubbles. Several AOIs in the study contained weather-related noise that made lateral stacking pollute the image blurring plume delineation that showed significant improvement in data quality when vertically stacked. Figure 32 shows an example of ghost plume visible in vertical stack and side-R-Stack. These ghost plumes are MBES fore-aft transmitter sidelobe artifacts created by strong scattering plumes that are difficult to map using geopicking (Figure 32 shows geopicks in blue) as well as using the Feature Detection toolkit in FMMidwater. For precision seep sampling, vertical stacking helps interpretation by flattening the acoustic artifacts into an along-track smear or cross with the emission site represented by the highest amplitude.

Conclusion

A multibeam data set containing more than 600 previously mapped plumes in the NGOM was reprocessed using a vertical stacking method to create 2D midwater amplitude maps. These maps were compared with the manually digitized points to evaluate mapping uncertainty between the existing qualitative midwater mapping technique and EI of midwater samples. The results show ranging discrepancies between the interpreted seafloor position of the geopicks and the amplitude anomalies indicating that the traditional manual digitizing of hydrocarbon plumes is not ideal for precision coring required in commercial seep hunting. Vertical stacking of midwater data shows a significant improvement in increasing the S/N over lateral stacking methods for enhanced localization of seafloor gas emission and improved geochemical coring. Vertical stacking midwater data can be automated and provides an objective and repeatable technique for processing and analysis of large volumes of MBES midwater data. Ultimately, this mapping method using a quantitative backscatter surface helps solve ambiguities in midwater interpretation for acquiring high-quality geochemical samples of seep sediments.

Acknowledgments

We thank Chuck Anderson and the NOAA National Center for Environmental Information in Boulder, CO for multibeam data accessibility; Geoffroy Lamarache, Peter Urban, and the Geohab Water Column Working Group for collaboration and inspiration; Jean Marie Augustin and Ifremer for SonarScope development and technical guidance; and NOAA's Office of Ocean Education along with the captain and crew of the NOAA Ship Okeanos Explorer onboard during EX1402. Lastly, we are indebted to Jens Greinert, Phil Teas, and one anonymous reviewer for their valuable comments and insight into improving this paper.

Raw MBES data were acquired from NOAAs Bathymetry Data Viewer hosted by NCEI in Boulder, CO (https://maps.ngdc.noaa.gov/viewers/bathymetry/). The BOEM Seismic Water Bottom Anomalies layer package can be accessed at https://www.boem.gov/oil-gas-energy/mapping-and-data/map-gallery/seismic-water-bottom-anomalies-map-gallery.

Data and materials availability

Data associated with this research are available and can be accessed via the following URL: https://maps.ngdc.noaa.gov/viewers/bathymetry.

References

Abrams, M. A., 1996, Distribution of subsurface hydrocarbon seepage in near-surface marine sediments, *in* D. Schumacher and M. A. Abrams, eds., Hydrocarbon migration and its near-surface expression: AAPG Memoir 66, 1–14.

Abrams, M. A., 2005, Significance of hydrocarbon seepage relative to petroleum generation and entrapment: Marine and Petroleum Geology, **22**, 457–477, doi: 10.1016/j.marpetgeo.2004.08.003.

Abrams, M. A., and N. F. Dahdah, 2011, Surface sediment hydrocarbons as indicators of subsurface hydrocarbons: Field calibration of existing and new surface geochemistry methods in the Marco Polo area, Gulf of Mexico: AAPG Bulletin, **95**, 1907–1935, doi: 10.1306/03211110130.

Augustin, J. M., 2011, Developing and deploying sonar and echosounder data analysis software: Matlab Newsletters, http://www.mathworks.fr/company/newsletters/articles/developing-and-deploying-sonar-andechosounder-data-analysis-software.html, accessed 29 June 2021.

Brewer, P. G., F. M. Orr, G. Friederich, K. A. Kvenvolden, and D. L. Orange, 1998, Gas hydrate formation in the deep sea: In situ experiments with controlled release of methane, natural gas, and carbon dioxide: Energy & Fuels, **12**, 183–188, doi: 10.1021/ef970172q.

Dragesund, O., and S. Olsen, 1964, On the possibility of estimating year-class strength by measuring echo-abundance of 0-group fish: ICES.

Dupré, S., C. Scalabrin, C. Grall, J. M. Augustin, P. Henry, A. C. Şengör, N. Görür, M. Çağatay, and L. Géli, 2015, Tectonic and sedimentary controls on widespread gas emissions in the Sea of Marmara: Results from systematic, shipborne multibeam echo sounder water column imaging: Journal of Geophysical Research, Solid Earth, **120**, 2891–2912, doi: 10.1002/2014JB011617.

Fisher, C., H. Roberts, E. Cordes, and B. Bernard, 2007, Cold seeps and associated communities of the Gulf of Mexico: Oceanography, **20**, 69–79, doi: 10.5670/oceanog.2007.12.

Frye, M., 2008, Preliminary evaluation of in-place gas hydrate resources: Gulf of Mexico Outer Continental Shelf, U.S. Dept. Interior, Minerals Management Service, Resource Evaluation Division: OCS Report MMS 2008-004.

Gee, L., L. McKenna, and J. Beaudoin, 2014, New tools for water column feature detection, extraction, and analysis — FMMidwater interactively visualizes time-varying geospatial data: Sea Technology, **55**, 27–30.

Innangi, S., A. Bonanno, R. Tonielli, F. Gerlotto, M. Innangi, and S. Mazzola, 2016, High resolution 3D shapes of fish schools: A new method to use the water column backscatter from hydrographic multibeam echo sounders: Applied Acoustics, **111**, 148–160, doi: 10.1016/j.apacoust.2016.04.017.

Jerram, K., T. C. Weber, and J. Beaudoin, 2015, Split-beam echo sounder observations of natural methane seep variability in the northern Gulf of Mexico: Geochemistry, Geophysics, Geosystems, **16**, 736–750, doi: 10.1002/2014GC005429.

Korneliussen, R. J., Y. Heggelund, I. K. Eliassen, O. K. Bye, T. Knutsen, and J. Dalen, 2009, Combining multibeam-sonar and multifrequency-echosounder data: Examples of the analysis and imaging of large euphausiid schools: ICES Journal of Marine Science, **66**, 991–997, doi: 10.1093/icesjms/fsp092.

Kramer, K. V., and W. W. Shedd, 2017, A 1.4-billion-pixel map of the Gulf of Mexico seafloor: Eos, **98**, doi: 10.1029/2017EO073557.

Lamarche, G., Y. Le Gonidec, V. Lucieer, Y. Ladroit, T. Weber, A. Gaillot, E. Heffron, S. Watson, and A. Pallentin, 2019, Gas bubble forensics team surveils the New Zealand ocean: Eos, **100**, doi: 10.1029/2019EO133649.

Leifer, I., and I. MacDonald, 2003, Dynamics of the gas flux from shallow gas hydrate deposits: Interaction between oily hydrate bubbles and the oceanic environment: Earth and Planetary Science Letters, **210**, 411–424, doi: 10.1016/S0012-821X(03)00173-0.

McConnell, D. R., and D. L. Orange, 2014, Are marine geochemical surveys unreliable? It is all about location: EAGE Shallow Anomalies Workshop, doi: 10.3997/2214-4609.20147423.

McKenna, L. A., 2014, Mapping data report, Cruise EX1402L2, Exploration mapping, Gulf of Mexico, Galveston, TX to Pascagoula, MS, March 19–April 4, 2014: National Oceanic and Atmospheric Administration, doi: 10.7289/V5F47M4D.

Mitchell, G. A., D. L. Orange, J. J. Gharib, and P. Kennedy, 2018, Improved detection and mapping of deepwater hydrocarbon seeps: Optimizing multibeam echosounder seafloor backscatter acquisition and processing techniques: Marine Geophysical Research, **39**, 323–347, doi: 10.1007/s11001-018-9345-8.

Nikolovska, A., H. Sahling, and G. Bohrmann, 2008, Hydroacoustic methodology for detection, localization, and quantification of gas bubbles rising from the seafloor at gas seeps from the eastern Black Sea: Geochemistry, Geophysics, Geosystems, **9**, doi: 10.1029/2008GC002118.

Orange, D. L., P. A. Teas, and J. Decker, 2010, Multibeam backscatter — Insights into marine geological processes and hydrocarbon seepage: Offshore Technology Conference, Extended Abstracts, doi: 10.4043/20860-MS.

Portell, J., D. Amblas, G. Mitchell, M. Morales, A. G. Villafranca, R. Iudica, and G. Lastras, 2019, High-performance compression of multibeam echosounders water column data: IEEE Journal of Selected Topics in Applied Earth Observations and Remote Sensing, **12**, 1771–1783, doi: 10.1109/JSTARS.2019.2915844.

Roberts, H. H., B. A. Hardage, W. W. Shedd, and J. Hunt Jr., 2006, Seafloor reflectivity — An important seismic property for interpreting fluid/gas expulsion geology and the presence of gas hydrate: The Leading Edge, **25**, 620–628, doi: 10.1190/1.2202667.

Römer, M., H. Sahling, T. Pape, G. Bohrmann, and V. Spieß, 2012, Quantification of gas bubble emissions from submarine hydrocarbon seeps at the Makran continental margin (offshore Pakistan): Journal of Geophysical Research, Oceans, **117**, C10, doi: 10.1029/2011JC007424.

Schneider von Deimling, J., J. Brockhoff, and J. Greinert, 2007, Flare imaging with multibeam systems: Data processing for bubble detection at seeps: Geochemistry, Geophysics, Geosystems, **8**, doi: 10.1029/2007GC001577.

Simmonds, J., and D. N. MacLennan, 2008, Fisheries acoustics: Theory and practice: John Wiley & Sons.

Skarke, A., C. Ruppel, M. Kodis, D. Brothers, and E. Noecker, 2014, Widespread methane leakage from the sea floor on the northern US Atlantic margin: Nature Geoscience, **7**, 657, doi: 10.1038/ngeo2232.

Trenkel, V. M., V. Mazauric, and L. Berger, 2008, The new fisheries multibeam echosounder ME70: Description and expected contribution to fisheries research: ICES Journal of Marine Science, **65**, 645–655, doi: 10.1093/icesjms/fsn051.

Urban, P., K. Köser, and J. Greinert, 2017, Processing of multibeam water column image data for automated bubble/seep detection and repeated mapping: Limnology and Oceanography: Methods, **15**, 1–21.

Wall, C. C., 2016, Building an accessible archive for water column sonar data: Eos, **97**, doi: 10.1029/2016EO057595.

Wall, C. C., J. M. Jech, and S. J. McLean, 2016, Increasing the accessibility of acoustic data through global access and imagery: ICES Journal of Marine Science, **73**, 2093–2103, doi: 10.1093/icesjms/fsw014.

Weber, T. C., L. A. Mayer, J. Beaudoin, K. Jerram, M. A. Malik, B. Shedd, and G. Rice, 2012, Mapping gas seeps with the deepwater multibeam echosounder on *Okeanos Explorer*: Oceanography, **25**, no. 1, doi: 10.5670/oceanog.2011.supplement.01.

Weber, T. C., L. Mayer, K. Jerram, J. Beaudoin, Y. Rzhanov, and D. Lovalvo, 2014, Acoustic estimates of methane gas flux from the seabed in a 6000 km^2 region in the Northern Gulf of Mexico: Geochemistry, Geophysics, Geosystems, **15**, 1911–1925, doi: 10.1002/2014GC005271.

Biographies and photographs of the authors are not available.

DOI:10.1190/INT-2021-0084.1